Chemosphere 263 (2021) 128030

Contents lists available at ScienceDirect

Chemosphere

journal homepage: www.elsevier.com/locate/chemosphere

Insights into size-segregated particulate chemistry and sources in urban environment over central Indo-Gangetic Plain

Nandita Singh [a], Tirthankar Banerjee [a, b, *], Vishnu Murari [a], Karine Deboudt [c], Md Firoz Khan [d], R.S. Singh [e], Mohd Talib Latif [f]

[a] Institute of Environment and Sustainable Development, Banaras Hindu University, Varanasi, India
[b] DST-Mahamana Centre of Excellence in Climate Change Research, Banaras Hindu University, Varanasi, India
[c] Laboratoire de Physico-Chimie de l'Atmosphère, Université du Littoral Côte d'Opale, Dunkerque, France
[d] Department of Chemistry, Faculty of Science, University of Malaya, Kuala Lumpur, Malaysia
[e] Department of Chemical Engineering and Technology, Indian Institute of Technology (BHU), Varanasi, India
[f] Department of Earth Sciences and Environment, Universiti Kebangsaan Malaysia, Bangi, Malaysia

HIGHLIGHTS

- Fine particulates were secondary in nature against metal enriched coarse particulates.
- Neutralization of particulate acidity varies in size-segregated particulates.
- Molecular distributions of organics indicate both biogenic & anthropogenic emissions.
- Secondary aerosols and biomass burning emissions are the dominant sources of $PM_{2.1}$.
- Both crustal resuspensions and secondary aerosols were responsible emitters of $PM_{>2.1}$.

GRAPHICAL ABSTRACT

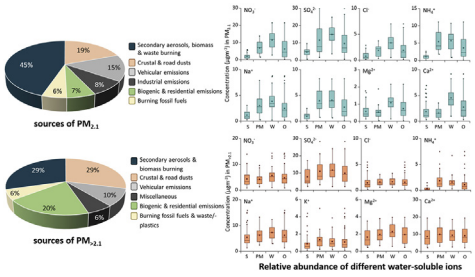

ARTICLE INFO

Article history:
Received 25 June 2020
Received in revised form
5 August 2020
Accepted 9 August 2020
Available online 19 August 2020

Handling Editor: Dr. R Ebinghaus

Keywords:
Aerosols
Levoglucosan
Organics
Receptor model
Secondary aerosols

ABSTRACT

Size-segregated airborne fine ($PM_{2.1}$) and coarse ($PM_{>2.1}$) particulates were measured in an urban environment over central Indo-Gangetic plain in between 2015 and 2018 to get insights into its nature, chemistry and sources. Mean ($\pm 1\sigma$) concentration of $PM_{2.1}$ was 98 (± 76) μgm^{-3} with a seasonal high during winter (DJF, 162 $\pm$ 71 μgm^{-3}) compared to pre-monsoon specific high in $PM_{>2.1}$ (MAMJ, 177 $\pm$ 84 μgm^{-3}) with an annual mean of 170 (± 69) μgm^{-3}. $PM_{2.1}$ was secondary in nature with abundant secondary inorganic aerosols (20% of particulate mass) and water-soluble organic carbon (19%) against metal enriched (25%) $PM_{>2.1}$, having robust signature of resuspensions from Earth's crust and road dust. Ammonium-based neutralization of particulate acidity was essentially in $PM_{2.1}$ with an indication of predominant H_2SO_4 neutralization in bisulfate form compared to Ca^{2+} and Mg^{2+}-based neutralization in $PM_{>2.1}$. Molecular distribution of *n*-alkanes homologues (C_{17}–C_{35}) showed C_{max} at C_{23} ($PM_{2.1}$) and C_{18} ($PM_{>2.1}$) with weak dominance of odd-numbered *n*-alkanes. Carbon preference index of *n*-alkanes was close to unity ($PM_{2.1}$: 1.4 $\pm$ 0.3; $PM_{>2.1}$: 1.3 $\pm$ 0.4). Fatty acids (C_{12}–C_{26}) were characterized with predominance of even carbon with C_{max} at n-hexadecanoic acid ($C_{16:0}$). Low to high molecular weight fatty acid ratio ranged from 2.0 ($PM_{>2.1}$) to 5.6 ($PM_{2.1}$) with vital signature of anthropogenic emissions. Levoglucosan was abundant in $PM_{2.1}$ (758 $\pm$ 481 ngm^{-3}) with a high ratio (11.6) against galactosan,

* Corresponding author. Institute of Environment and Sustainable Development, Banaras Hindu University, Varanasi, India.
E-mail addresses: tb.iesd@bhu.ac.in, tirthankaronline@gmail.com (T. Banerjee).

https://doi.org/10.1016/j.chemosphere.2020.128030

emphasizing robust contribution from burning of hardwood and agricultural residues. Receptor model resolves secondary aerosols and biomass burning emissions (45%) as the most influential sources of $PM_{2.1}$ whereas, crustal (29%) and secondary aerosols (29%) were found responsible for $PM_{>2.1}$; with significant variations among the seasons.

1. Introduction

Airborne particulates are inextricably linked with many adverse human health and environmental impacts and therefore, have been studied extensively in terms of their sources (Belis et al., 2013; Chakraborty et al., 2015; Jain et al., 2020), composition (Weagle et al., 2018; Ren et al., 2016; Singh et al., 2018), spatial (Giles et al., 2011; Mhawish et al., 2017, 2020; Sen et al., 2017) and temporal variations (Jethva et al., 2005; Kumar et al., 2018), climatic implications (Ramanathan et al., 2001) and health impacts (Lelieveld et al., 2015). However, proper quantification of particulates' feedback to climate system and human health pose considerable uncertainties. This is especially due to the variation in particulate types and by the influences of local/-regional meteorology which facilitate particulate and its precursors to continuously evolve while being airborne (Jimenez et al., 2009; Seinfeld et al., 2016; Singh et al., 2017a). Ideally, the nature of airborne particulates is the function of its sources (like combustion sources, crustal sources, marine aerosols etc.) which govern its fundamental properties especially size, morphology, composition and thereby, possible implications to receptor site. Therefore, to establish adverse impacts of airborne particulate with high level of certainty, and to improvise an effective air quality management plan; it is absolutely necessary to identify particulate sources and variations, both in terms of space and time.

Entire South Asia has been well documented as one of the most densely populated and highly polluted region, having two third of world's critically polluted cities (iqair.com/world-most-polluted-cities). Within the sub-continent, the Indo-Gangetic Plain (IGP) shares the maximum burden of air pollution with diverse kind of sources that too typically vary with seasons (Banerjee et al., 2015; Singh et al., 2017a,b). However, lack of proper ground-based monitoring network often limits the fundamental understanding of the nature of pollution and extent of human exposure. Likewise, in India, population-weighted average distance to the nearest air quality monitor is > 70 km and there is approximately a single monitor for each 7 million people (Martin et al., 2019). Besides, all the monitoring stations are essentially located in urban agglomerates therefore, comparison of polluted cities against background concentration is hardly feasible. Sources of airborne fine particulate matter ($PM_{2.5}$) have been explored across IGP, like in Lahore (Rasheed et al., 2015), Delhi (Jain et al., 2020; Sharma et al., 2016), Agra (Kulshrestha et al., 2009), Kanpur (Villalobos et al., 2015), Kolkata (Chowdhury et al., 2007) and in Dhaka (Begum et al., 2004). However, the central part of IGP is relatively less explored in terms of the sources of fine particulates, although there are instances when sources of coarser (PM_{10}, Shukla and Sharma, 2008; Murari et al., 2020) and submicron aerosols were investigated (PM_1, Chakraborty and Gupta, 2010; Singh and Gupta, 2016; Chakraborty et al., 2015). Most of these studies conclude biomass burning emissions, vehicular sources and secondary aerosols as dominant contributors to PM_1 mass, with significant seasonal variations;

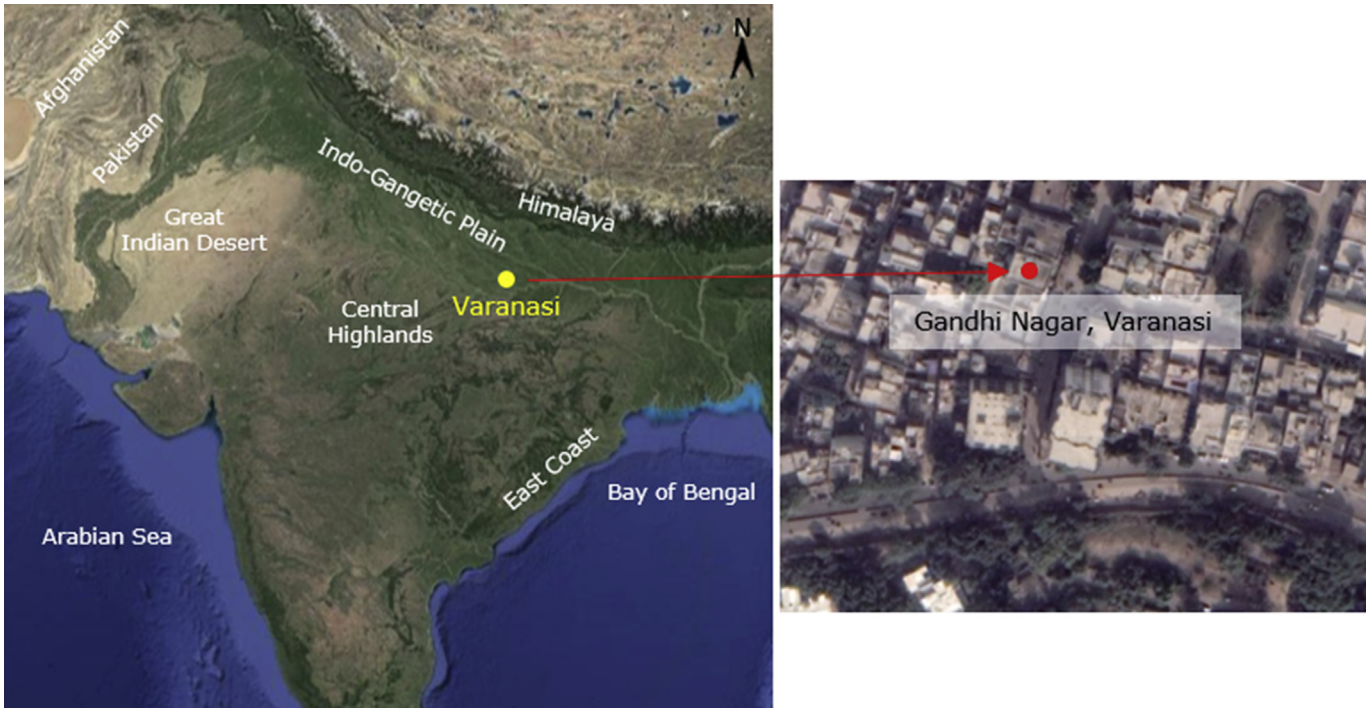

Fig. 1. Geographical location of the particulate monitoring station.

while crustal resuspensions primarily contribute to the PM_{10} mass. However, almost none of the researches across IGP took size-segregated aerosols as matrix thereby a large void of knowledge remains. Besides, central IGP also holds the characteristics in accumulating particulates from the upper IGP and north-western dry regions, facilitated mainly by the westerly wind (Sen et al., 2017; Kumar et al., 2018; Murari et al., 2020) and an anti-cyclonic zone of subsidence prevailing over the region (Dey and Di Girolamo, 2011; Singh et al., 2018). All these factors essentially led to a mixed kind of particulates which necessitates systematic investigation of particulate chemistry, sources and transport to establish its possible health and climatic implications over the region.

In the present study, size-segregated particulate mass has been monitored continuously for three years (October 2015–June 2018) in an urban background in Varanasi, an air pollution hotspot over central IGP. Size-segregated fine ($PM_{2.1}$) and coarse particulates ($PM_{>2.1}$) were speciated initially to characterize water-soluble ions, organic compounds and elements constrained by different seasons. New insights on particulate chemistry have been explored in terms of variations in secondary inorganic aerosols, ionic balance and neutralization of particulate acidity in size-segregated aerosols. Factors that drive the seasonal variations in particulate chemistry and molecular distribution of organics have also been assessed. Sources relevant to the particulate were detected and quantified using positive matrix factorization receptor model following several established organic and inorganic markers. Potential transport of airborne particulates across IGP was identified and relative contributions of different source regions were quantified. Implications of this research may be to improve parametrization of regional air quality model as particulate chemistry and source apportionment of size-segregated aerosols has been rare across the IGP. Besides, new insights on particulate chemistry will help to strengthen regional air quality management plan and to relate source specific impacts of particulates to human health and changing climate.

2. Experimental location and data analysis

2.1. Study area

Particulates were monitored in a residential premise in Gandhi Nagar (25°25′ N, 82°99′ E, 82.2 m above sea level), located at 2 km south of the city center in Varanasi (Fig. 1). The monitoring location represents a typical residential area with potential emission sources like road traffic, resuspensions of road dust, crustal soil/dust and biomass/-waste incineration. No major industrial emissions contribute exclusively to the local particulate loading except contribution from few small-scale manufacturing industries, food and metal processing industries. However, there are evidences that prevailing westerly typically contribute to local pollution by accumulating particulates from upper part of IGP, frequently during pre-monsoon (MAMJ; Sen et al., 2017; Dey et al., 2004), post-monsoon (ON; Singh et al., 2018) and in winter seasons (DJF; Kumar et al., 2017). The station experiences humid tropical climate with no localized effect of ocean and/-or mountain. However, convective movement of airborne particulates to upper height is crucial as the region experiences considerable diurnal variation in boundary layer that facilitate dispersion of pollutants at a higher height (Murari et al., 2017; Vinjamuri et al., 2020).

2.2. Monitoring of airborne particulates

Size-segregated particulate was monitored once in a week continuously for 72 h for a period of three years (October 2015 to June 2018; N: 112) except in monsoon seasons (July–September). Anderson eight-stage cascade impactor (Tisch Environmental Inc., USA) having aerodynamic cut-off diameter of <0.43, 0.65, 1.1, 2.1, 3.3, 4.7, 5.8 and > 9.0 μm with 50% collection efficiency was used to monitor particulates using pre-combusted quartz fiber filter (Whatman, UK). For each sample, individual stages were segregated into two groups: (i) coarse mode ($PM_{>2.1}$) combining all the stages with the aerodynamic diameter >2.1 μm and (ii) fine mode ($PM_{2.1}$) for the stages with diameter <2.1 μm. Filters were subject to desiccate pre-and post-sampling and stored under cool and dry conditions (relative humidity: 45 ± 5%). Mass concentrations were calculated gravimetrically using an analytical microbalance (AY220, Shimadzu).

2.3. Particulate speciation

2.3.1. Trace metals

Metallic species associated with particulate were analyzed following US EPA Method IO-3.2 (EPA, 1999). Exposed filters were digested for 2 h in an extracting solution (5.55% HNO_3 with 16.67% HCl) and filtered (Whatman No. 42). Final filtrate was diluted and used to analyze for metallic species (Ca, Mg, Na, K, Fe, Zn, Mn, Pb, Ni, Cu, Cr, Co, Cd) by inductively coupled plasma optical emission spectrometer (iCAP 6300 DUO, Thermo Scientific). The three-point calibration was performed for individual metal with certified reference material and blank correction was made. Standard recovery tests were done and recovery efficiencies among the metals varied from 93% (Cu) to 100% (Ni).

2.4. Organic compounds

Filter composites were used to measure aerosol organic constituents. Quartz filters were ultrasonicated for 30 min initially with dichloromethane-hexane mixture (1:1), followed by dichloromethane-methanol mixture (1:1). Extracts were concentrated using a vacuum rotatory evaporator and nitrogen evaporator to a volume of 100 μL (Hu et al., 2013), before being derivatized (silylation) with N,O-bis-(trimethylsilyl)-trifluoroacetamide and 1% trimethylchlorosilane. Residue was re-dissolved in hexane and was used to analyze organic components by a gas chromatograph-mass spectrometer (GCMS-QP2010 Ultra, Shimadzu, Japan). The GCMS was equipped with Rxi-5MS fused silica capillary column (30 m × 0.25 mm ID x 0.25 μm; Restek, Bellefonte, PA, USA). Injector temperature was set at 260 °C in splitless mode. The GCMS oven temperature was set at 50 °C with 2 min of the isothermal hold. This has followed by raising temperature to 120 °C (linear elevation at 30 °C min^{-1}) and 300 °C (linear elevation at 6 °C min^{-1}) with a final isothermal hold of 11 min. The electron impact ionization was used to produce molecular ions at 70 eV with temperature maintained at 230 °C and 270 °C, for ion source and interface, respectively. The molecular ions were scanned for a wide range (*m/z*: 40 to 650). Target species were identified following the retention time and fragmentation pattern available from NIST library (National Institute of Standards and Technology) and standard solution of analytes. The average recoveries (respective RSD) of the 19 n-alkanes varied from 72 to 92% (1–12%), 75–88% (2–7%) for 5 phthalates, 74–92% (1–9%) for fatty acid methyl-esters, 74–92% (3–5%) dicarboxylic acids and 75–80% (4–6%) for anhydrosugars. Both field and laboratory blank filters undergone the identical procedure as the exposed samples for quality assurance.

2.5. Water-soluble inorganic species (WSIS)

Water-soluble inorganic species (WSIS) were analyzed using an

Ion Chromatograph (ICS-3000, Dionex, USA). Exposed filters were cut into pieces and WSIS were extracted through ultra-sonication (90 min) in deionized water having resistivity of 18.2 MΩcm. The aqueous solutions were then filtered through 0.2 μm pore size syringe filters. Anions (Cl^-, NO_3^- and SO_4^{2-}) were estimated using an anion micro-membrane suppressor (AERS-300, 4 mm; Dionex) with IonPac (AS11-HC × 250-mm) analytical column and guard column IonPac (AG11-HC, 4 × 50 mm; Dionex). The eluent used for anion analysis was 20 mM NaOH (50% w/w). Cations (Na^+, K^+, NH_4^+, Mg^{2+} and Ca^{2+}) were separated using a suppressor (CERS-300, 4 mm; Dionex) with an analytical column (IonPac CS12A-HC, 4 × 250 mm; Dionex) and a guard column (IonPac CG11-HC, 4 × 50 mm; Dionex), with 5 mM MSA (methane sulphonic acid) as eluent (Murari et al., 2015).

2.6. Water-soluble organic carbon (WSOC)

The extract prepared for WSIS analysis was additionally used to measure particulate-bound water-soluble organic carbon (WSOC). Both blank and sample solutions were analyzed for WSOC using Total Organic Carbon Analyzer (TOC-1200, Thermo ECN Corp.) following the protocol by Kirillova et al. (2010).

2.7. Source apportionment of particulate

Source apportionment of particulate was achieved by multivariate factor analysis simulated through USEPA Positive Matrix Factorization (PMF 5.0, Paatero and Tapper, 1994). The PMF detects particulate sources and quantify their contributions on the basis of weighted least square approach (Khan et al., 2016; Cesari et al., 2018). The PMF requires a large dataset to effectively apportion a source while it has limitations in terms of its inability to separate covariant sources, rotational uncertainty and sensitivity to model pre-set parameters (Banerjee et al., 2015). The PMF relate each factor (p), the particulate source profile (f) and the individual source contribution (g) to each sample and can be expressed as:

$$x_{ij} = \sum_{k=1}^{p} g_{ik} f_{kj} + e_{ij} \quad (1)$$

where, i is the considered sample, j is the considered chemical species and x_{ij} refers to the concentrations associated to the i by j matrix and e_{ij} denotes species residuals. Uncertainty in data was adjusted accordingly to retain maximum dataset for the model. The uncertainty (U) associated with each species measurement above

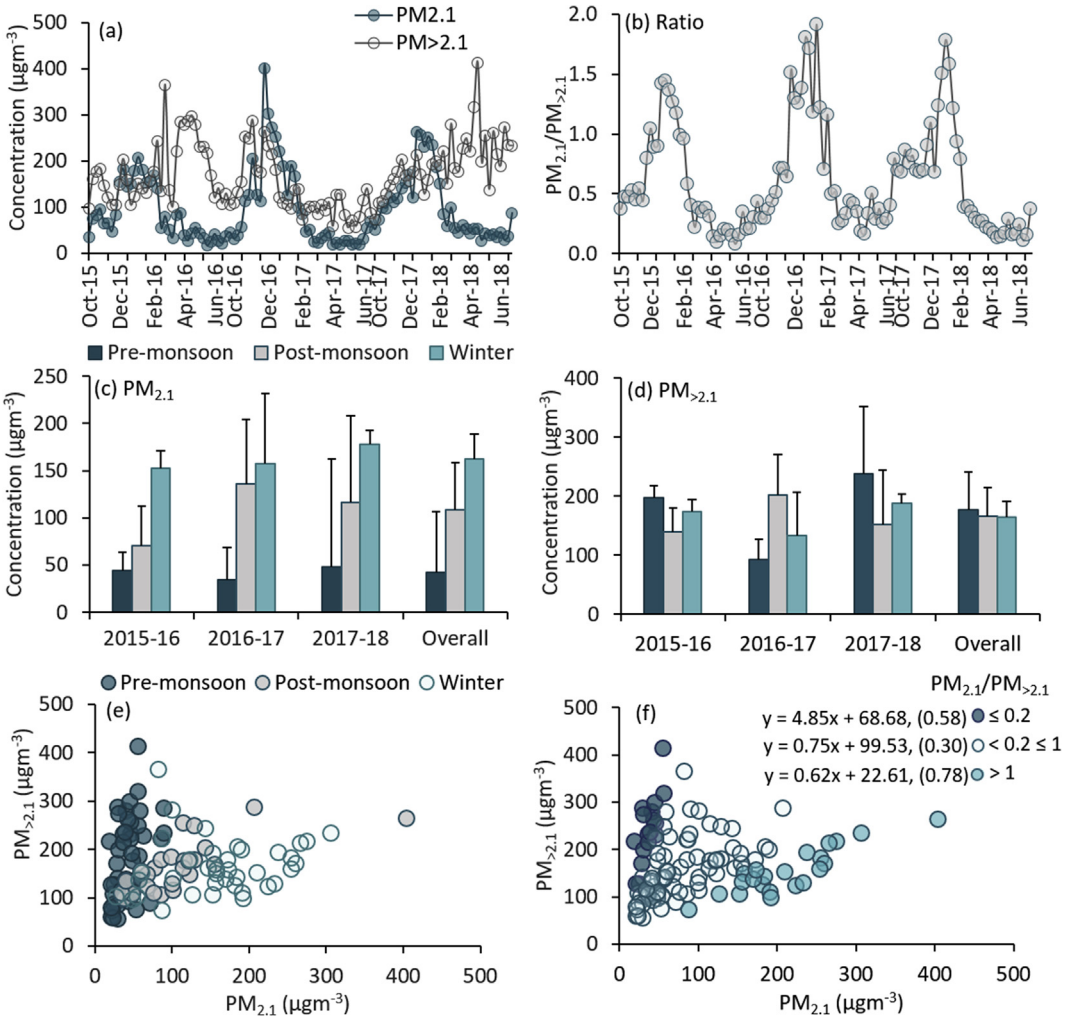

Fig. 2. Temporal variation in (a) size-segregated particulate mass concentration, (b) $PM_{2.1}$ on $PM_{>2.1}$ concentration ratio, (c) seasonal variation in each monitoring year in $PM_{2.1}$ and (d) in $PM_{>2.1}$, (e) $PM_{>2.1}$ as a function of $PM_{2.1}$ and (f) scatter plot of the $PM_{2.1}$ on $PM_{>2.1}$ concentration ratio.

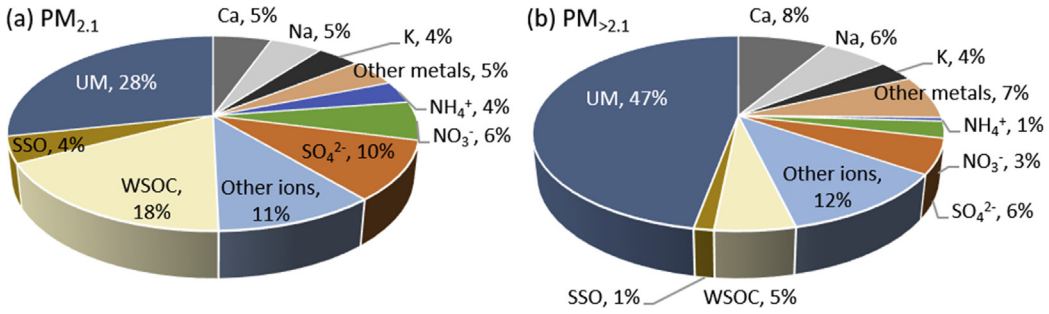

Fig. 3. Relative composition of airborne (a) fine and (b) coarse particulates. N**OTE**. UM: unmeasured; SSO: solvent-soluble organics; WSOC: water-soluble organic carbon.

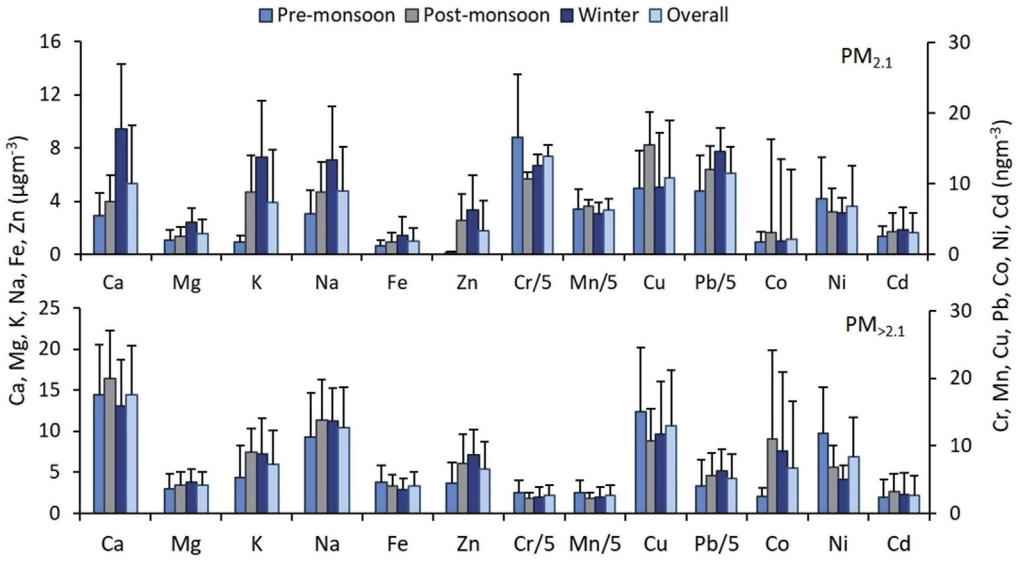

Fig. 4. Seasonal variations in element species in fine and coarse particulates.

method detection limit (MDL) was estimated using equation (2):

$$U = \sqrt{(error\ fraction\ \mathrm{x}\ concentration)^2 + (0.5\ x\ MDL)^2} \qquad (2)$$

where, error fraction is the percentage of uncertainty in the data. The MDL was calculated as 3σ of the sample blanks and species with concentrations below MDL was replaced with the half of the MDL value (Khan et al., 2016). Any missing value was replaced with corresponding species median and uncertainty was put as four-times the species median. Based on signal (S) to noise (N) ratio, the species were considered as 'strong' if S/N > 2, 'weak' if 0.2 < S/N ≤ 2 and 'bad' if S/N ≤ 0.2. Particulate mass concentration was put as 'weak' so that it does not influence the model performance. A total of 112 samples with 13 particulate-bound metallic species, 8 WSIS, 2 anhydrosugars, 19 *n*-alkanes, 5-phthalates, 3-dicarboxylic acids and 12 fatty acids were used as input to simulate source contribution. The PMF analysis was performed with a model uncertainty of 5% and various number of factors (3–7) were tested. Six factors showed a reasonable physical interpretation and residuals were well distributed in almost all the variables between −3 and 3. The selection of appropriate markers for different sources is one of the fundamental steps in particulate source apportionment. In absence of local source profile, identification and selection of source-specific markers was based on available literature (e.g. Banerjee et al., 2015; Viana et al., 2008; Pant and Harrison, 2012). Table S1 enlists the chemical species that were considered as molecular markers of individual source. Due to spatial heterogeneity in particulate sources and temporal variations in emission source strengths across the IGP, markers were selected which were only true representative of associated sources and were only relevant to the monitoring location.

2.8. Particulate transport and source fields

To simulate possible transport of air mass, five-days (120 h) air mass back trajectories at 500 m and 1500 m (AMSL) were plotted using NOAA HYSPLIT model (Draxler and Rolph, 2003). The HYSPLIT was run based on Global Data Assimilation System data (GDAS, 0.5 ° × 0.5 °) archived at http://ready.arl.noaa.gov/gdas1.php. Air-mass back trajectories (00:00, 06:00, 12:00 and 18:00 UTC) were made using GIS-based software TrajStat (Wang et al., 2009). Air masses were also subject to cluster and potential source contribution function (PSCF) analysis to delineate the spatial distribution of potential aerosol sources and to estimate their contributions. Specificities of the models' parameters and algorithms are detailed in Wang et al. (2009) and Kumar et al. (2018).

3. Results and discussion

3.1. General characteristics of particulate

Seventy-two hours mean fine ($PM_{2.1}$) and coarse ($PM_{>2.1}$) particulate concentration time-series from October 2015 to June 2018

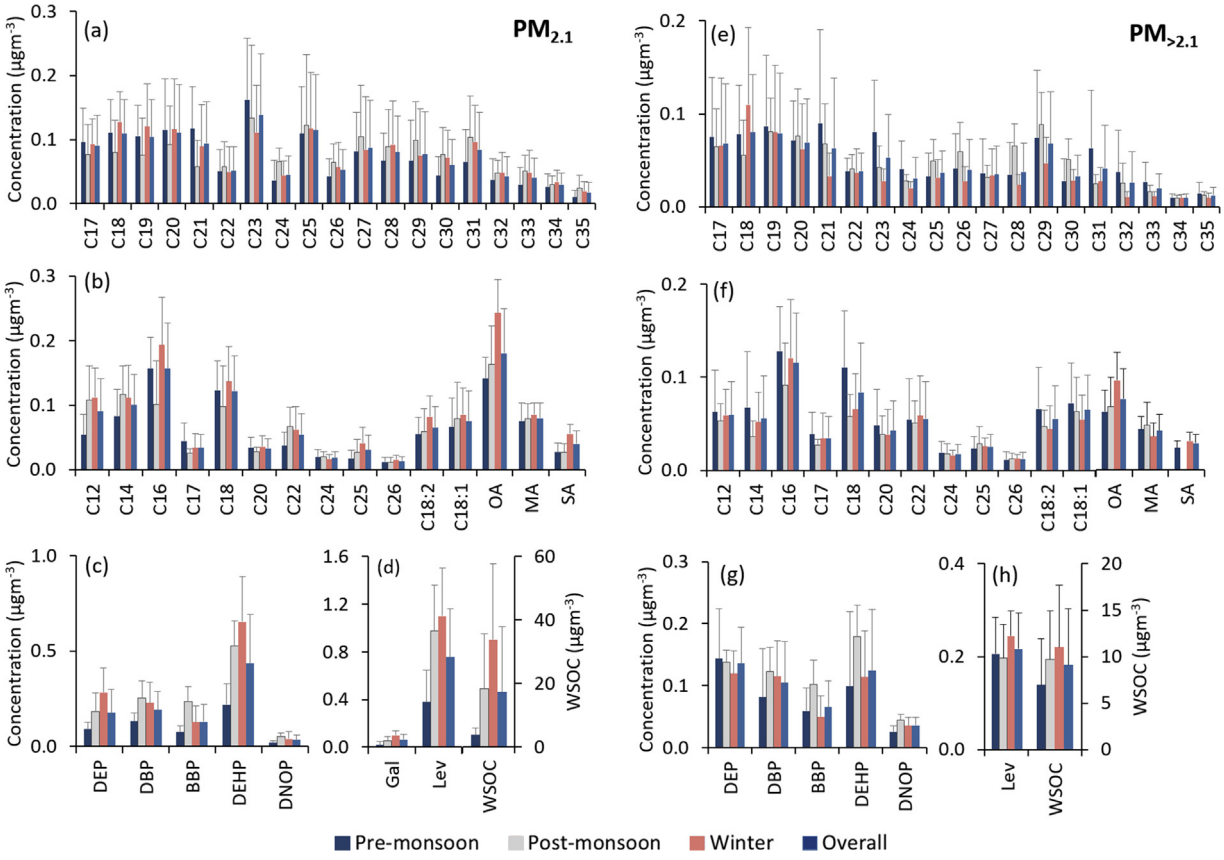

Fig. 5. Molecular distribution of *n*-alkanes (a,e), fatty acids and dicarboxylic acids (b,f), phthalates (c,g), anhydrosugars and WSOC (d,h) in fine (a–d) and coarse particulates (e–h). **NOTE**. For abbreviation please follow Table S4.

(N: 112) is presented in Fig. 2a with descriptive statistics included in Table S2 (a,b). Temporal trend in particulate concentration is clearly evident as coarse particulate escalates during month of April to May with a second peak in December till February, whereas fine particulates peak only during November to February months. Average (±1σ) mass concentration of $PM_{2.1}$ was 98 (±76) µgm^{-3}, with a seasonal high during winter (162 ± 71 µgm^{-3}; Fig. 2c) followed by post-monsoon (109 ± 73 µgm^{-3}) while, relative abundance of $PM_{2.1}$ reduced during pre-monsoon season (42 ± 17 µgm^{-3}). Approximately 76% of the monitoring events exceeded the 24-hourly national standard ($PM_{2.5}$: 40 µgm^{-3}) clearly indicating a chronic risk of exposure to the urban population, which was exacerbated during post-monsoon and winter months with 48% (in ON) to 76% (in DJF) of monitoring events surpassing 100 µgm^{-3}. Coarse particulates also showed seasonality in mass concentration (median: 159; range: 57–414 µgm^{-3}) however, less stringent relative to its counter-part; with highest concentration during pre-monsoon (177 ± 84 µgm^{-3}; Fig. 2d) and no clear distinction in between winter (165 ± 58 µgm^{-3}) and post-monsoon months (166 ± 53 µgm^{-3}). Overall mean (±SD) $PM_{>2.1}$ concentration was 170 (±69) µgm^{-3} with 88% of monitoring events exceeding 100 µgm^{-3}.

Total particulate loading (∑all the stages in impactor) has also significant inter-seasonal variations (median: 273; range: 81–669 µgm^{-3}) with a major contribution from the coarse mode particles ($PM_{>2.1}$: 66 ± 16%; $PM_{2.1}$: 34 ± 16%). During pre-monsoon, 79% (±8%) of total particulate loading was attributed to coarse particles whereas, contribution of fine particles maximized during winter (48 ± 13%). This is also apparent in fine to coarse particulate ratio time-series (Fig. 2b) with a clear decline in pre-monsoon (mean ± SD: 0.3 ± 0.1; range: 0.1–0.8) compared to the overall mean (0.6 ± 0.5). Particulate ratio in contrast, increased sharply during winter months (1.0 ± 0.5) with 58% of monitoring events register a $PM_{2.1}$:$PM_{>2.1}$ ratio >1, signifying exceedance in fine particulate concentration (Fig. 2e). Such incidences with very high R^2 (0.78; Fig. 2f) refer the contribution from similar kind of sources. In post-monsoon, particulate ratio varied in between 0.3 and 1.5 (mean ± SD: 0.6 ± 0.3) indicating co-dominance of $PM_{2.1}$ and $PM_{>2.1}$. Our previous findings based on both ground (Sen et al., 2014, 2017; Murari et al., 2017) and satellite-based observations (Kumar et al., 2015) also substantiate the fact that during post-monsoon and winter, there is a greater accumulation of fine particles across central Gangetic plain, where otherwise mixed type of particulates dominate.

3.2. Relative composition of fine and coarse particulates

Relative compositions of airborne fine and coarse particulates are shown in Fig. 3 while seasonal discrepancies are included in Fig. S1 (supplementary file). Water-soluble inorganic species (WSIS, all cations and anions) contributed major fraction of fine particulates mass (32 ± 11%) which varied non-significantly in between the seasons (31–34%). Sulfate was the most abundant species among the WSIS contributing 10% of $PM_{2.1}$ followed by nitrate, attributing 6% of $PM_{2.1}$ mass (Fig. S2). Contribution of secondary inorganic aerosols (SIAs, sulfate, nitrate, and ammonium) to total WSIS ranged in between 43% ($PM_{>2.1}$) and 63% ($PM_{2.1}$). The SIA accounted for 20% (18%–22%) of $PM_{2.1}$ mass indicating secondary nature of particulate origin, in accordance to the reported observations across IGP (Sharma et al., 2016; Singh et al., 2018; Jain et al.,

2020). Particulate-bound elements contributed nearly 19% of the $PM_{2.1}$ mass, without much variations in between the seasons (17–21%). Among the elements, crustal originated species like Ca (5%) and Na (5%) dominate the contribution followed by K (4%). Water-soluble organic carbon (WSOC) was largely associated to fine particulate (mean ± SD: 18 ± 7%) varying disproportionately among the seasons (9–21%). A higher fraction of $PM_{2.1}$ bound WSOC particularly during winter (21 ± 7%) also serves a crucial signature of the contribution of biomass burning emissions.

Coarse particulates, in contrast were found to be less secondary with SIA contributing 10% (7–12%) of $PM_{>2.1}$ mass (Fig. 3), primarily associated to sulfate (6%) and nitrate ions (3%). Besides, contributions of Ca^{2+} (5%) and Na^{+} ions (4%) were noted which were otherwise low (<3%) in abundance in $PM_{2.1}$ mass. WSIS constituted nearly 22% (±7%) of $PM_{>2.1}$, however varying considerably in between the seasons (17–25%). Coarse particulates were strongly metal enriched (25%) primarily having the species of crustal origin (Ca, Na and Zn), with robust seasonal variations (22–29%). The WSOC fraction was relatively low in coarse particulate (5 ± 3%) without no such seasonal predominance.

3.2.1. Elements

Seasonal variations in individual particulate-bound element species are shown in Fig. 4. In both size fractions, the most abundant species were Ca and Na, contributing nearly 55–58% of total quantified metal concentration, while the remaining fraction was mainly composed of K, Mg and Zn (34–39%). Coarse particulates were enriched in Ca (8.5%) and Na (6.1%) accounting 15% of particulate mass, slightly high during post-monsoon season (Ca: 9.9%; Na: 6.9%). Association of Ca and Na in particulate invariably suggest the contribution of re-suspension of crustal materials like bare soils and/-or road dust by local winds. Other metallic species with crustal signature (like Mg and Fe) also denote higher fractional contribution in coarse particulate mass (4.0%) compared to finer one (2.6%). Natural sources of Fe include earth's crusts and road dust resuspensions; however presence of Fe in $PM_{2.1}$ possibly indicate contribution from vehicular sources (non-exhaust emissions like tire and brake wear; Banerjee et al., 2015; Kukutschová et al., 2011). Potassium (K) was the third most abundant species both in $PM_{2.1}$ (4.0%) and $PM_{>2.1}$ (3.5%); particularly from post-monsoon to winter (4.3–4.5%) compared to pre-monsoon months (2.2–2.5%). This may be an indication of added contribution from burning of biomass, residual oil, refuse and garbage (Singh et al., 2018). Another important species found abundant in airborne particulate was Zn accounting 1.8% ($PM_{2.1}$) to 3.2% ($PM_{>2.1}$) of particulate mass. Zinc was high particularly in coarse particulate having typical non-exhaust emissions from vehicles and from burning of residual oil (Gonzalez et al., 2016); while high abundance during post-monsoon to winter ($PM_{2.1}$: 4.3–4.5%; $PM_{>2.1}$) irrespective of particulate size may also be an indication of contribution from tire wear, burning of waste refuse and garbage (Kumar et al., 2017; Banerjee et al., 2015). Among the trace heavy metals, Pb (0.06 ± 0.03 μgm^{-3}) and Cr (0.07 ± 0.03 μgm^{-3}) was found to enrich <0.2% of fine particulate mass, indicating a possible contribution of anthropogenic sources, especially from the metal processing and manufacturing industries.

3.3. Organic compounds

Homologous series of 19 n-alkanes (C_{17}–C_{35}), 12 fatty acids (C_{12}–C_{26}), 3 dicarboxylic acids (oxalic acid, malonic acid, succinic acid), 5 phthalates and 2 anhydrosugars were detected in size-segregated aerosols in Varanasi. Variations in individual organic component and their molecular distributions are shown in Fig. 5, the summary of the concentrations and diagostic ratios are presented in Table S3 and all abbreviations are included in Table S4.

n-Alkanes. Average (±SD) concentration of *n*-alkanes was high in fine particulates (1430 ± 737 ngm^{-3}) compared to coarser one (842 ± 490 ngm^{-3}). Concentration noted in Varanasi is considerably high compared to other Indian cities like in Delhi (204 ngm^{-3}, Gadi et al., 2019; 681 ngm^{-3}; Kang et al., 2016), Raipur (150 ngm^{-3}; Giri et al., 2013) and Kanpur (16–79 ngm^{-3}; Villalobos et al., 2015) but very high concentrations were also reported globally (Santiago, 5400 ngm^{-3}; Didyk et al., 2000). Molecular distribution of homologous *n*-alkanes showed C_{max} at C_{23} ($PM_{2.1}$) and C_{18} ($PM_{>2.1}$) with a weak dominance of odd-numbered *n*-alkanes in both low (LMW, $<C_{25}$) and high molecular weight alkanes (HMW). Besides, in both types of particulate, concentration of LMW *n*-alkanes with sources like burning of fossil fuels, remain 1.8 to 2.0 times higher than the HMW *n*-alkanes having biogenic sources like epicuticular wax (for $PM_{>2.1}$), and biomass burning emissions (for $PM_{2.1}$). The discrepancies were particularly high in pre-monsoon (2.2–2.3) compared to post-monsoon months (1.1–1.3). For both $PM_{2.1}$ and $PM_{>2.1}$, CPI remain close to unity ($PM_{2.1}$: 1.4 ± 0.3; $PM_{>2.1}$: 1.3 ± 0.4) especially during post-monsoon (1.2–1.4) and winter (1.1–1.3), indicating the dominance of petrogenic emissions like incomplete combustion of fossil fuels and petroleum residues (Singh et al., 2018; Ren et al., 2016).

Fatty acids. Fatty acids (C_{12}–C_{26}) including two unsaturated fatty acids (oleic acid, $C_{18:1}$ and linoleic acid, $C_{18:2}$) were quantified. Fatty acids constitute a greater fraction of solvent extractable organics within the fine mode (756 ± 234 ngm^{-3}) compared to the coarse mode aerosols (620 ± 265 ngm^{-3}), with no robust seasonal preference except moderate enhancement during winter (only in $PM_{2.1}$: 926 ± 193 ngm^{-3}) and pre-monsoon (in $PM_{>2.1}$: 701 ± 329 ngm^{-3}). Both biogenic (plant fatty acids e.g. foliar vegetation combustion, waxy leaf surface abrasions, and wood smoke) and anthropogenic sources (vehicular exhausts, residential cooking and biomass burning) are responsible emitters of fatty acids, but biogenic emissions are mostly HMW fatty acids ($\geq C_{20}$) while LMW fatty acids are essentially anthropogenic (Fu et al., 2011; Ren et al., 2016). Here, LMW to HMW fatty acids ratio range in between 2.0 (±2.9) in $PM_{>2.1}$ and 5.6 (±2.9) in $PM_{2.1}$, indicating vital signature of anthropogenic emission sources.

Molecular distribution of fatty acids is characterized by a strong prevalence of even carbon both in $PM_{2.1}$ and $PM_{>2.1}$ with C_{max} at n-hexadecanoic acids ($C_{16:0}$), followed by n-octadecanoic acids ($C_{18:0}$). This is well identical to the reported observation from Raipur (Giri et al., 2013), Chennai (Fu et al., 2010), New Delhi (Gadi et al., 2019) and Beijing (Ren et al., 2016) but different from the bimodal distribution ($C_{16:0}$ and $C_{24:0}/C_{28:0}$) noted in mountain and marine aerosols (Fu et al., 2011; Ren et al., 2016). The ratio of $C_{18:0}$ to $C_{16:0}$ serves as an indicator of potential sources of fatty acids, with $C_{18:0}/C_{16:0}$ <0.25 refer biogenic emissions, 0.25–0.50 as vehicular emissions and values beyond 0.50 indicate emissions from residential cooking and from paved and unpaved road dust (Rogge et al., 2006). We noted a mean value close to 0.9 both in $PM_{2.1}$ (0.91) and $PM_{>2.1}$ (0.87), similar to the urban aerosols reported in Beijing (Ren et al., 2016). Unsaturated fatty acids (UFA; $C_{18:n}$ and $C_{16:1}$) are mainly fresh biogenic and marine/microbial origin (Fu et al., 2013) while vehicular emissions, cooking and solid biomass burning also emit UFA. Being very reactive, UFA readily convert to saturated mono- and dicarboxylic acids ($C_{(18:0+16:0)}$) in the atmosphere though process known as oxidative cleavage (Kawamura and Gagosian, 1987). Therefore, ratio between $C_{(18:0+16:0)}$ and $C_{(18:n+16:1)}$ (C_{sat}/C_{unsat}) serves as an essential indicator of atmospheric aging of organic aerosols. Here, C_{sat}/C_{unsat} remain in between 1.3 ($PM_{2.1}$) and 1.7 ($PM_{>2.1}$); with slight prevalence of saturated against unsaturated fatty acids referring contribution of both local and

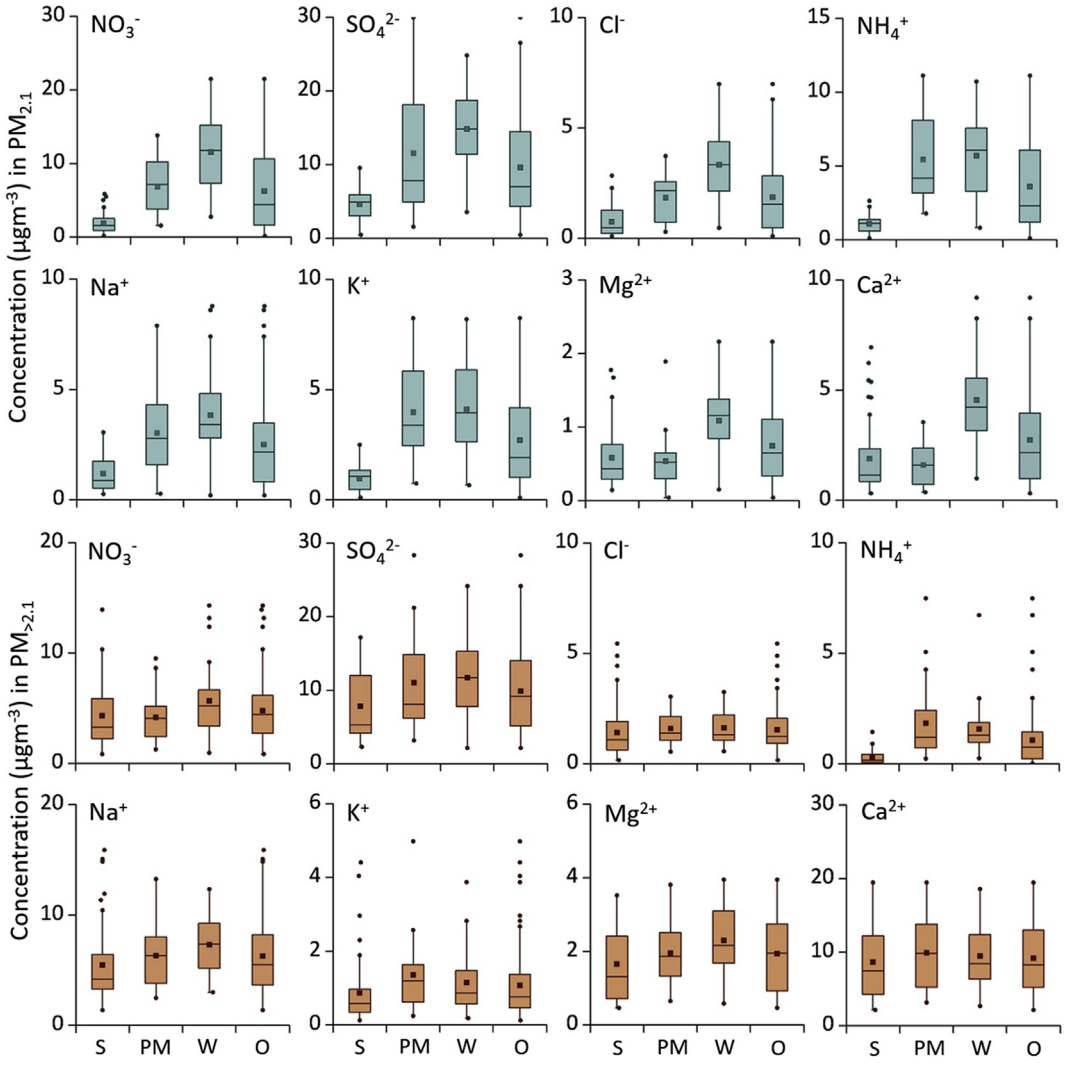

Fig. 6. Intra-seasonal variations in particulate-bound ions in fine and coarse particulates. **NOTE**. S = Pre-monsoon (MAMJ), PM = Post-monsoon (ON), W = Winter (DJF) & O = Overall (all months except JAS).

transported aerosols.

Dicarboxylic acids (DCA). DCA are the water-soluble organic compounds that acts as cloud-condensation nuclei. They originate primarily from the burning of biomass and bio-fuels, vehicular emissions and oceans, but photo-chemical oxidations of volatile organic compounds (VOCs) also generate DCA (Sorathia et al., 2018). Here, mean (±SD) DCA concentration (C_2, C_3 and C_4) was high in fine particulates (299 ± 106 ngm^{-3}) compared to coarse one (122 ± 46 ngm^{-3}); that too typically elevated during peak biomass burning period ($PM_{2.1}$, ON: 287 ± 115; DJF: 390 ± 82 ngm^{-3}). Our observation was low compared to those reported in Kanpur (1499 ± 562 ngm^{-3}) possibly because Sorathia et al. (2018) considered C_2 to C_{10} DCA bound in PM_{10} measured during peak biomass burning period (DJF). However, in accordance to other reported observations like in Sorathia et al. (2018), Kawamura and Yasui (2005) and Pavuluri et al. (2010); greater abundance of oxalic acid (C_2) followed by succinic acid (C_4) and the malonic acid (C_3) was found. The C_2 was characteristically high in fine particulates during winter ($PM_{2.1}$: 246 ± 64; $PM_{>2.1}$: 97 ± 30 ngm^{-3}) compared to its annual mean ($PM_{2.1}$: 187 ± 74; $PM_{>2.1}$: 76 ± 32 ngm^{-3}), accounting 50–60% of total measured DCA concentration. Our observation is lower than the reported PM_{10} bound C_2 concentration in New Delhi (~1400 ngm^{-3}; Miyazaki et al., 2009) and Kanpur (1390 ngm^{-3}; Sorathia et al., 2018) but comparable to those in Chennai (435 ngm^{-3}; Pavuluri et al., 2010) and Tokoyo (357 ngm^{-3}; Kawamura and Yasui, 2005).

Phthalates. Major sources of particulate-bound phthalates include burning of plasticizers including softeners, antioxidants and initiators; however it may also be emitted from vehicular exhaust, industrial emissions, from burning of waste including plastics, plasticizer formulation used in fertilizers and insecticides, or by emissions of vinyl chloride and other volatile compounds (Giri et al., 2013; Gadi et al., 2019). Five types of phthalates including Diethyl phthalate (DEP), Di-butyl phthalate (DBP), Butyl benzyl phthalate (BBP), Bis(2-ethylhexylphthalate) (BEHP), Di-n-octyl phthalate (DnOP) were detected both in $PM_{2.1}$ and $PM_{>2.1}$. Phthalates ($\sum$5P) were abundant in the fine fractions (965 ± 504 ngm^{-3}) compared to the coarser one (468 ± 220 ngm^{-3}). It also exhibits a noticeable increase during winter (1331 ± 482 ngm^{-3}) and post-monsoon (1249 ± 319 ngm^{-3}), precisely in the fine fractions while there was no seasonal predominance in $PM_{>2.1}$. Concentration measured in Varanasi was comparable to those reported at Raipur (2–926 ngm^{-3}; Giri et al., 2013) and New Delhi (130–210 ngm^{-3}; Gadi et al., 2019). Molecular distribution among

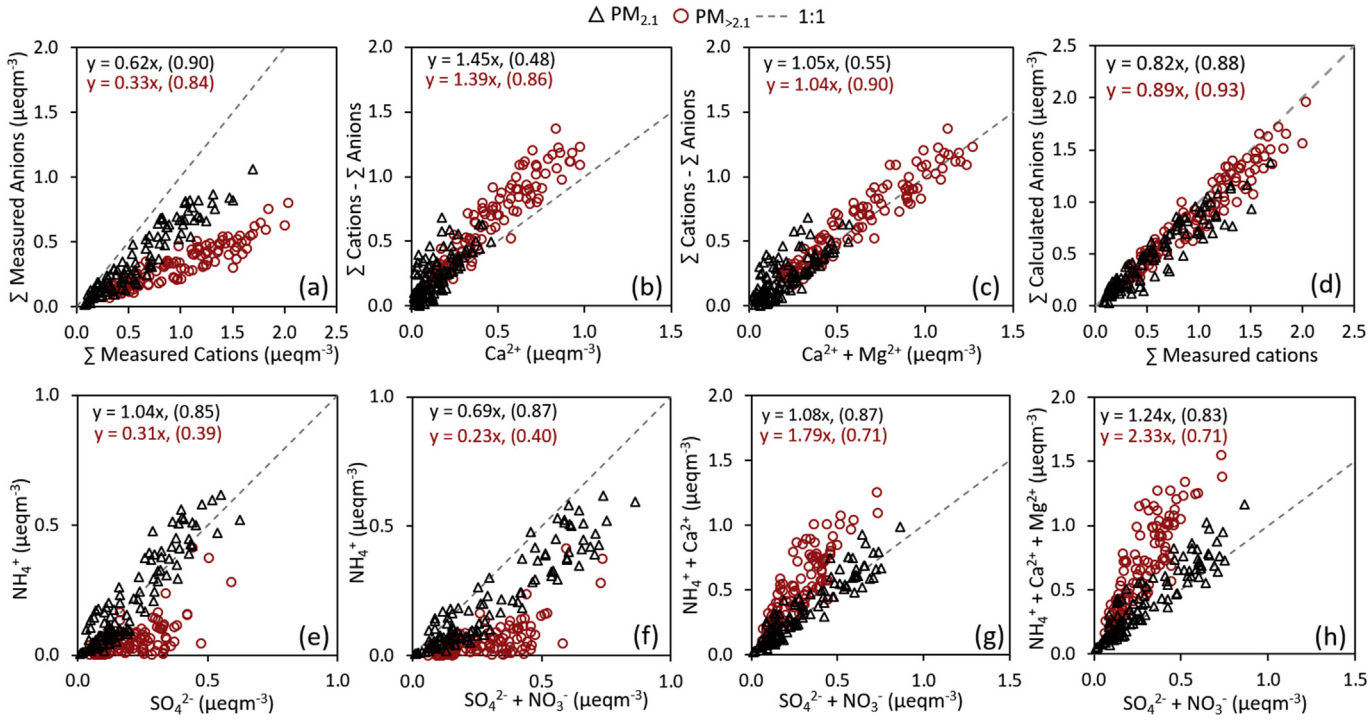

Fig. 7. Ionic balance in size-segregated particulates (a) measured total anions versus total cations, (b) anion deficiency against Ca^{2+}, (c) anion deficiency against Ca^{2+} and Mg^{2+}, (d) reconstructed anions against measured cations, and neutralization of particulate acidity (e) NH_4^+ against SO_4^{2-}, (f) NH_4^+ against SO_4^{2-} and NO_3^- (g) NH_4^+ and Ca^{2+} against SO_4^{2-} and NO_3^- and (h) NH_4^+, Ca^{2+}, Mg^{2+} against SO_4^{2-} and NO_3^-.

the phthalates indicates BEHP (435 ± 258 ngm^{-3}) as the most abundant species in $PM_{2.1}$, accounting 50% of total phthalates while, both DBP (129 ± 65 ngm^{-3}) and BEHP (124 ± 98 ngm^{-3}) were prevalent in the coarse fraction. A similar distribution was also evident in Delhi by Gadi et al. (2019) referring to the use of BEHP in PVC, cosmetic products, coatings and varnishes and their burning emissions as potential sources of airborne phthalates.

Anhydrosugars. Among the anhydrosugars, levoglucosan was present both in fine and coarse particulates whereas, its isomer galactosan was only detected in the fine fractions and mannosan remained untracable. Levoglucosan primarily emits from the combustion of cellulose and hemicellulose and accepted universally as biomarker of biomass burning emissions (Cheng et al., 2013; Singh et al., 2018; Banerjee et al., 2015). Fine particulates were rich in levoglucosan (758 ± 481 ngm^{-3}); particularly in post-monsoon (979 ± 381 ngm^{-3}) and winter months (1101 ± 405 ngm^{-3}), with relative abundance comparable to other reported observations across IGP e.g. in New Delhi (1978 ngm^{-3}; Li et al., 2014), Kanpur (1363–1853 ngm^{-3}; Sorathia et al., 2018) and in other Asian cities e.g. Lumbini, Nepal (734 ngm^{-3}, Wan et al., 2017) and Beijing, China (590 ngm^{-3}, Cheng et al., 2013). Presence of levoglucosan was earlier traced in Varanasi in fine particulates (ON: 878 ngm^{-3}; Singh et al., 2018) during peak biomass burning period however, mainly concentrated (~75%) in submicron particulates. A ratio of levoglucosan to its isomer was also used to discriminate the types of biomass burning, with a ratio <10 for softwood combustion and >10 for burning of hardwood and crop residues (Cheng et al., 2013). Galactosan, an isomer of levoglucosan, was high in winter (100 ± 40 ngm^{-3}) compared to its annual mean (65 ± 48 ngm^{-3}). Levoglucosan to galactosan mean ratio remain 11.6 and essentially peaked in post-monsoon (17.4); emphasizing robust contribution from the burning of hardwood and agricultural residues. Since 80% of anhydrosugars remain in the fine fractions, a relatively low abundance of levoglucosan in $PM_{>2.1}$ (217 ± 77 ngm^{-3}) was expected without much seasonal variations.

WSOC. The WSOC contributed significantly to fine particulate (18 ± 7%) compared to coarse particulate mass (5 ± 3%). Daily variation in WSOC was high in $PM_{2.1}$ (1–85 μgm^{-3}), with very high wintertime concentration (34 ± 24 μgm^{-3}); whereas no such seasonality was noted for $PM_{>2.1}$ (Table S2). A significant association was also noted in between WSOC and levoglucosan (R^2: 0.6), K^+ (R^2: 0.64), and oxalic acid (R^2: 0.6) in $PM_{2.1}$ indicating their common source of origin including biomass burning and atmospheric oxidation of VOCs (Miyazaki et al., 2009).

3.3.1. Water-soluble inorganic species (WSIS)

Fig. 6 illustrates the intra-seasonal variations in particulate-bound ion concentration against their respective means. Fine particulates were enriched in sulfate and nitrate accounting 16% of $PM_{2.1}$ mass (Fig. S2); while rest of the ions (like NH_4^+, Na^+, Ca^{2+} and K^+) altogether contribute 12%. Similarly, sulfate was also the species contributing maximum mass fraction to the coarse particulate (6%), followed by however, crustal species like Ca^{2+} (5%) and Na^+ (4%); and contribution of NO_3^- remained <3%. Sulfate in $PM_{2.1}$ reached its peak during winter months (14.8 ± 4.9 μgm^{-3}) without any meaningful variations in particulate mass fraction throughout the year (9.1–10.9%). The trend was similar for $PM_{>2.1}$ with highest concentration also in winter (11.7 ± 5.2 μgm^{-3}) while mass fraction reduced considerably during pre-monsoon (4.4%) against post-monsoon (6.7%) and winter (7.1%). Incidentally, intra-seasonal variation in SO_4^{2-} was highest during post-monsoon both in $PM_{2.1}$ (SD: ±8.5 μgm^{-3}) and $PM_{>2.1}$ (SD: ±6.4 μgm^{-3}), with seasonal mean ($PM_{2.1}$: 11.8; $PM_{>2.1}$: 11.0 μgm^{-3}) considerably high compared to its median ($PM_{2.1}$: 7.8; $PM_{>2.1}$: 8.1 μgm^{-3}); which was possibly due to the varying strength of biomass burning emissions over the region (Singh et al., 2018; Kaskaoutis et al., 2014). Nitrate was the second most abundant species in $PM_{2.1}$, noted strongly during winter (11.6 ± 4.6 μgm^{-3}); whereas $PM_{>2.1}$ was partially devoid of nitrate

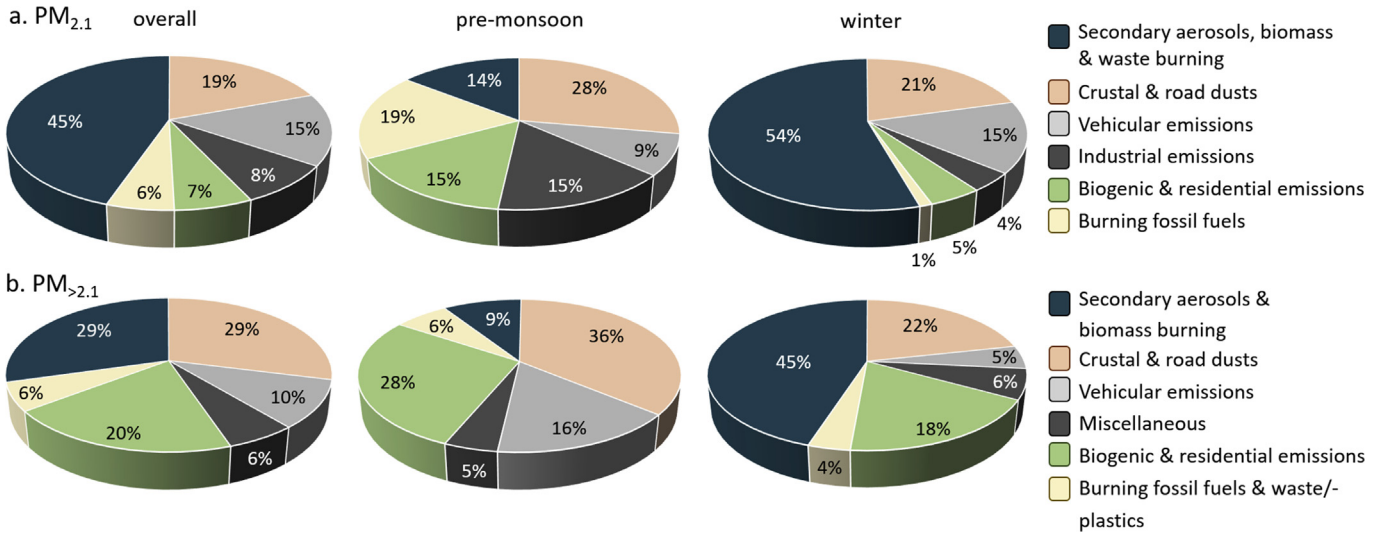

Fig. 8. Relative contributions of various emission sources to $PM_{2.1}$ and $PM_{>2.1}$.

($4.7 \pm 2.8\ \mu gm^{-3}$), with less stringent variation within the season. This may indicate that $PM_{>2.1}$ bound nitrate was associated to a more consistent source type and strength, like vehicular emissions while in $PM_{2.1}$, it may also be influenced by intermittent contributions from biomass burning emissions. The $PM_{2.1}$-bound NO_3^-/SO_4^{2-} ratio varied from 0.40 (pre-monsoon) to 0.78 (winter), referring dominance of stationary sources over mobile sources (Tian et al., 2016). A ratio >1 was however, noted only during post-monsoon to winter months, an interlude often accounted with many hazy days; similar to the reported haze events over Guangzhou (Tan et al., 2009), Suzhou, China (Tian et al., 2016) and in Varanasi (Singh et al., 2018).

Particulate-bound ammonium (NH_4^+) showed highest enrichment in fine particulates ($3.6 \pm 3.1\ \mu gm^{-3}$) and contributed 4% of $PM_{2.1}$ mass; especially in post-monsoon (5%) compared to 0.6% (0.2–1.1%) mass fraction in $PM_{>2.1}$. Ammonium is an established marker of biomass burning emissions (Bray et al., 2018) and has been reported to enrich primarily in fine particulate (Singh et al., 2018; Tian et al., 2016). Besides, NH_4^+ has also sources like agricultural practices, livestock emissions, transport and industrial emissions. Other ionic species like Na^+ and Ca^{2+} was high in $PM_{>2.1}$ (Na^+: 6.3 ± 3.2; Ca^{2+}: $9.2 \pm 4.6\ \mu gm^{-3}$) compared to $PM_{2.1}$ (Na^+: 2.5 ± 2.0; Ca^{2+}: $2.7 \pm 2.1\ \mu gm^{-3}$), referring their possible origin from resuspensions of crustal dust/-soils. The K^+, also an important tracer of biomass burning emissions, was highly enriched in fine particulate ($2.7 \pm 2.2\ \mu gm^{-3}$); especially during post-monsoon ($4.0 \pm 2.2\ \mu gm^{-3}$) and winter ($4.1 \pm 2.0\ \mu gm^{-3}$), contributing up to 3% of $PM_{2.1}$ mass. Relative abundance of Cl^- in both size fractions was roughly equal, constituting 1–2% of particulate mass; slightly high in abundance in the fine fractions ($1.9 \pm 1.6\ \mu gm^{-3}$) compared to the coarse one ($1.5 \pm 1.0\ \mu gm^{-3}$). Possible origin of Cl^- in the coarse fraction could be the aged sea salt coming from Bay of Bengal, while emissions from biomass and waste/refuse burning mainly contribute to the fine fraction.

3.4. Ionic balance and neutralization of particulate acidity

Ionic equivalence of total anions (NO_3^-, SO_4^{2-}, Cl^-) against total cations (NH_4^+, Ca^{2+}, Mg^{2+}, Na^+, K^+) denote a strong correlation (R^2; $PM_{2.1}$: 0.90; $PM_{>2.1}$: 0.84) which indicate that all the measured WSIS were major species and they coexisted in airborne particulates (Fig. 7a). However, slope of the regression line was less than the unity and the anion deficiency (∑cations - ∑anions) was high in $PM_{>2.1}$ (slope: 0.33) compared to $PM_{2.1}$ (slope: 0.62). Anion deficiency in coarse particulate related strongly with Ca^{2+} (R^2: 0.86; Fig. 7b) and that too improved when an aggregate of Ca^{2+} and Mg^{2+} were considered (R^2: 0.90; Fig. 7c), but not in fine particulates possibly due to unassessed H^+ anions (Theodosi et al., 2011). The strong correlation of $[Ca^{2+} + Mg^{2+}]$ with anionic deficiency suggests CO_3^{2-} and HCO_3^- are the possible missing anions in $PM_{>2.1}$. Missing total CO_3^{2-} concentration was therefore, calculated following Querol et al. (2001) considering an aggregate of carbonate salt of Ca^{2+} (i.e. $1.5Ca^{2+}$) and Mg^{2+} (i.e. $2.5Mg^{2+}$) in equal proportions. The resulting correlations in between calculated anions (including CO_3^{2-}) and measured cations show significant improvement (R^2: 0.88–0.93) and slope near to unity which essentially validate that CO_3^{2-} was in fact a major anion missing both in $PM_{>2.1}$ and in $PM_{2.1}$ (Fig. 7d). A strong correlation between Ca^{2+} and Mg^{2+} ($R^2_{2.1}$: 0.61; $R^2_{>2.1}$:0.66) also suggest their common origin. Mean $[Cl^-]/[Na^+]$ ratios ($PM_{>2.1}$: 0.16 ± 0.07; $PM_{2.1}$: 0.54 ± 0.33) were however, largely deviated from the sea salt ratio (1.18; Seinfeld and Pandis, 2016), indicating insignificant influence of marine aerosol to measured WSIS.

Fig. 7(e-h) illustrates the possible neutralization mechanism of major acidic species (SO_4^{2-} & NO_3^-) in $PM_{2.1}$ and $PM_{>2.1}$. A strong correlation (R^2: 0.85) and a ratio close to unity (slope: 1.04) between NH_4^+ and SO_4^{2-} indicate complete neutralization of $PM_{2.1}$ bound acidic species by NH_4^+, whereas NH_4^+ was insufficient to neutralize SO_4^{2-} in $PM_{>2.1}$ (R^2: 0.39; slope: 0.31; Fig. 7e). As we combine NO_3^- with SO_4^{2-}; slope decreases in both size fractions (Fig. 7f), suggesting neutralization of NO_3^- by other basic ions in $PM_{>2.1}$, but a strong correlation in $PM_{2.1}$ (R^2: 0.87) indicates the formation of NH_4NO_3, particularly in the fine fraction. However, a ratio less than unity also suggests besides NH_4NO_3, nitrate may also present in other chemical forms. The neutralization factor (NF; Table S5) of NH_4^+ was higher than Ca^{2+} (1–3 times) and Mg^{2+} (3–10 times) during winter and post-monsoon season, indicating the predominate NH_4^+ neutralization in $PM_{2.1}$; whereas in pre-monsoon, Ca^{2+} (NF; $Ca^{2+} = 1.6 * NH_4^+$) was the predominant neutralizing species along with NH_4^+ and Mg^{2+} ions. Unlike $PM_{2.1}$, vary high NF of Ca^{2+} (5–19 times) and Mg^{2+} (2–6 times) than NH_4^+ were noted in $PM_{>2.1}$ which refer acidic species were mainly neutralized by crustal species *viz.* Ca^{2+} and Mg^{2+}. This was also evident in Fig. 7(g-h) in the correlation analysis of $[Ca^{2+} + NH_4^+]$

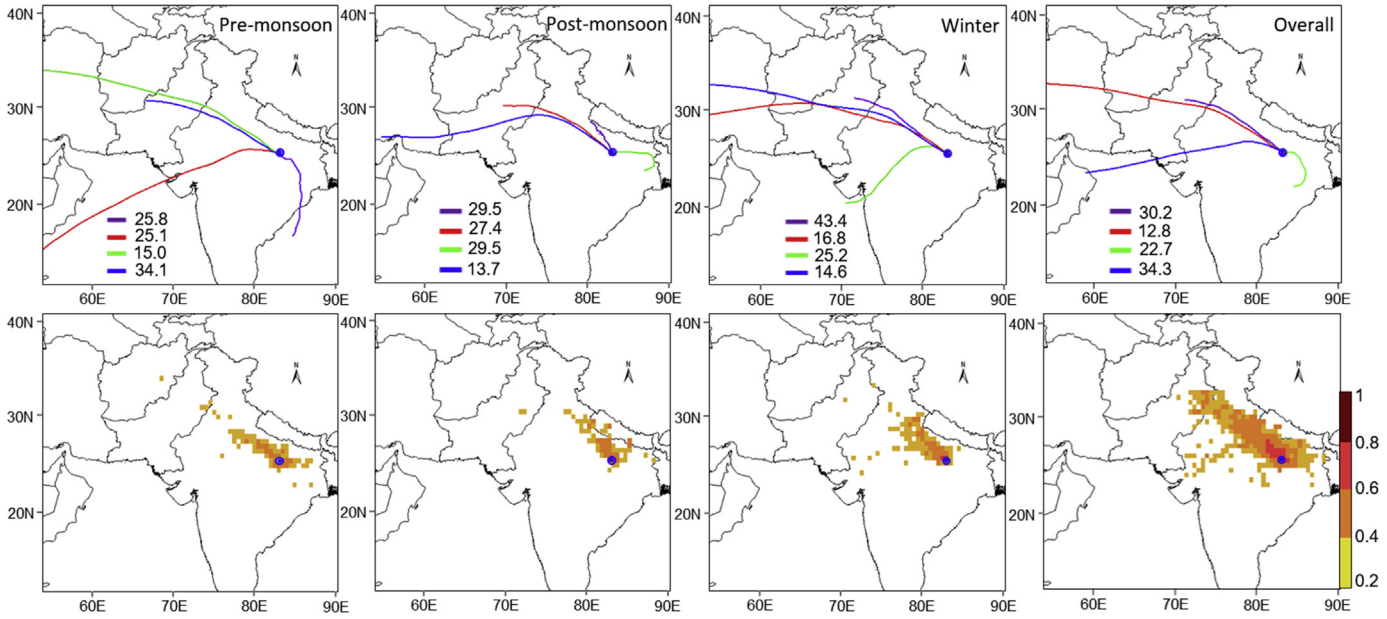

Fig. 9. Cluster of air mass backward trajectories and potential particulate source fields.

and $[NH_4^+ + Ca^{2+} + Mg^{2+}]$ against $[SO_4^{2-} + NO_3^-]$. The strong correlation and increased slope (>1) between $[Ca^{2+} + NH_4^+]$ and $[SO_4^{2-} + NO_3^-]$ therefore, suggest the formation of $Ca(NO_3)_2$ and $Mg(NO_3)_2$.

The neutralization in $PM_{2.1}$ showed a close association of NH_4^+ with SO_4^{2-} and NO_3^- in the form of $(NH_4)_2SO_4$ or NH_4HSO_4 and NH_4NO_3. Thermodynamically, reaction of SO_3 with NH_3 and H_2O is irreversible and favoured due to less energy barrier (Chen et al., 2018). Therefore, it was safe to assume that the NH_3 preferably neutralizes H_2SO_4 by forming $(NH_4)_2SO_4$ or NH_4HSO_4. To evaluate most suitable combination of SO_4^{2-} and HSO_4^- existence, the NH_4^+ was calculated following Chow et al. (1996) and ratio of calculated and measured NH_4^+ was adjusted for best fit close to 1. The estimated NH_4^+ in the form of $(NH_4)_2SO_4$ was higher than measured one (slope: 1.39) whereas the NH_4^+ in NH_4HSO_4 form was found lower than the measured concentration (slope: 0.93; Fig. S3). Thus, the best correlation (close to 1:1) was obtained for a combination of 80% NH_4HSO_4 and 20% $(NH_4)_2SO_4$ (slope: 1.02), suggesting that in $PM_{2.1}$ predominant H_2SO_4 neutralization possibly occurred in bisulfate form.

3.5. Identification of particulate source

Responsible sources of fine and coarse particulates in Varanasi were identified (Fig. 8) considering pre-selected particulate monitoring and speciation database measured from 2015 to 2018 (N: 112). Diverse kind of sources were identified, varying considerably in strength between the seasons both for $PM_{2.1}$ and $PM_{>2.1}$. Inorganic and biomolecular tracers of individual sources is included in Table S1 and the source factor profiles are shown in Figs. S4(a–b).

Overall, secondary aerosols and biomass burning emissions emerged out to be the most significant and highest contributing source (45%) to fine particulates, with higher contribution during winter (54%) compared to pre-monsoon months (14%). Contribution of secondary aerosols and biomass burning emissions were traced by the presence of secondary inorganic ions, WSOC, DCA and anhydrosugars; all showed a higher mass fraction during winter. Possible precursors to these secondary aerosols may be numerous (e.g. SO_2, NO_2, NH_3, VOCs) and both homogeneous gas-phase reactions and heterogeneous transformations contribute to the formation of these secondary aerosols. This factor also poses signature of waste burning emissions; as in Varanasi, often solid waste/-refuse and plastic are dumped and incinerated at road side along with dry plant debris and woods (Murari et al., 2020). Crustal resuspensions including resuspended road dust by local winds were the second important source (19%) to contribute into fine particulate that too increased during pre-monsoon (28%) compared to winter (21%). Vehicular emissions, including both tailpipe and non-exhaustive emissions contributed 15% (9–15%) of $PM_{2.1}$ while, emissions from burning of fossil fuels contributed 6% of fine particulate mass, with a peak during pre-monsoon months (19%). Another important source that emerged out was biogenic (vegetative detritus, epicuticular wax, waxy leaf surface abrasions, foliar vegetation combustion and wood smoke) and residential emissions (wood/-cow dung cake based residential cooking and heating) commonly practiced by several street food vendors and local inhabitants; contributing 7% of fine particulate mass.

Coarse particulates ($PM_{>2.1}$) were noted to be both crustal and secondary in origin as both the sources individually contribute 29% of particulate mass. The contribution of crustal sources especially resuspensions from the bare land surfaces and road dust by local wind enhanced particularly during pre-monsoon (36%) while, secondary aerosols including emissions from biomass burning were the prominent sources during winter (45%). Like in $PM_{2.1}$, $PM_{>2.1}$ also contained a robust signature of biogenic sources (20%) and residential emissions, with seasonal variations ranging from 18% (in winter) to 28% (in pre-monsoon). One typical and imperious source of particulates in pre-monsoon was the combine contribution of residential emissions and burning of fossil fuels, contributing 34% of particulate mass. This may typically include brick kilns emissions, which are mostly active during pre-monsoon and normally use diverse fuels (biomass, fossils fuels, kerosene, waste plastics, coal and crop residues) with minimum to no-emission control measures (Murari et al., 2020). The rest of the sources including vehicular emissions (10%); burning of fossil fuels, waste/-refuse, waste plastics (6%) and miscellaneous sources (6%) overall contribute <22% of particulate mass.

The nature and contribution of individual sources of airborne

particulates in Varanasi are comparable to that of reported observation across IGP. In most of the cases, crustal resuspensions, secondary aerosols and biomass burning are reported as the main sources of coarse particulates (Shukla and Sharma, 2008; Sharma et al., 2014; Murari et al., 2020). In contrast, fine particulates are often reported to be originated from vehicular emissions, biomass burning emissions and secondary aerosols (Singh et al., 2018; Jain et al., 2020; Kulshrestha et al., 2009), with considerable spatio-temporal variations among the monitoring stations. However, by using organic and inorganic tracers we were able to identify the contribution of several sources including biogenic and residential emissions, waste plastics and brick kilns with reduced uncertainty, which should be helpful in prioritizing air quality management plan for the region.

3.6. Particulate source field and transport

To better understand the possible origin of airborne particulates and transport through prevailing air mass, 5-days air-mass back-trajectories were plotted using HYSPLIT at 500 and 1500 m AMSL (Fig. 9). Annually two important clusters were recognized. One prevailing from north-western dry regions originating from upper IGP including northern parts of Pakistan, Punjab (India) and western semi-arid region contributing 30%; while the second important cluster (34%) originates from far west, including western India, lower Pakistan peninsula, parts of Middle-east and from Arabian sea. Both clusters possibly exerted significant impact to local particulate loading. In comparison, cluster originating from far east was less contributory in modifying regional air quality. Interestingly, the predominant clusters also remain consistent during post-monsoon and winter, with high contribution (85%) from north-west dry regions including upper IGP. The PSCF reciprocates the contribution of predominate clusters identifying the upper IGP as the most important source region for aerosols transported to central IGP. Overall, PSCF clearly indicates the significance of prevailing westerly in accumulating airborne particulates in the central IGP region, which has also been reported by contemporary researchers using both by ground- (Sen et al., 2017) and satellites-based observation (Kumar et al., 2018; Mhawish et al., 2020).

4. Conclusions

Three years of size-segregated particulate monitoring data was systematically analyzed to establish its nature, chemistry, sources and transport. We note that the monitoring location in central IGP remained far off from meeting air quality standard as 76% of the monitoring events exceeded the national standard while 88% of $PM_{>2.1}$ concentrations have exceeded 100 μgm^{-3}. Fine to coarse particulate ratio vary with time as $PM_{>2.1}$ dominated during pre-monsoon while $PM_{2.1}$ increased during winter. Chemical characterization of particulates revealed that fine particulates were mainly secondary in nature as secondary inorganic aerosols and water-soluble organic carbon dominated. In contrast, coarse particulates were primarily metal enriched, especially by the presence of species of crustal origin.

The $PM_{2.1}$-bound NO_3^- to SO_4^{2-} ratio indicate the dominance of stationary over mobile sources during pre-monsoon which were otherwise higher than unity during hazy days. Possible origin of different water-soluble ions was established. A robust association and a ratio close to unity in between NH_4^+ and SO_4^{2-} refer to the complete neutralization of $PM_{2.1}$ acidity by NH_4^+. In contrast, neutralization of acidic species in $PM_{>2.1}$ were mainly by the crustal species. Possible mechanism of NH_4HSO_4 and NH_4NO_3 formation in $PM_{2.1}$ were compared against the formation of $Ca(NO_3)_2$ and $Mg(NO_3)_2$ in $PM_{>2.1}$. Molecular distribution of *n*-Alkanes (C_{17}—C_{35}) were characterized with weak dominance of odd-numbered carbon whereas, predominance of even carbon was noted in fatty acids (C_{12}—C_{26}). The LMW to HMW ratio in both, *n*-alkanes and fatty acids indicate vital signature of anthropogenic origin. Among the dicarboxylic acids, oxalic acid was highly abundant in fine particulates, similar to the phthalates. High abundance of particulate-bound organics in fine particulate during winter were associated to the escalated anthropogenic emissions; especially from the burning of biomass/-waste/-refuse coupled with residential emissions while in coarse particulate, biogenic emissions also found to contribute significantly. Contribution of biomass burning emissions in $PM_{2.1}$ were further established by the presence of anhydrosugars.

Possible sources of airborne particulates were resolved using advanced receptor model considering several inorganic and bio-molecular tracers. Six predominate sources were identified for both $PM_{2.1}$ and $PM_{>2.1}$, and considerable seasonal deviations in their contributions were noted. Overall, secondary aerosols and biomass (including waste) burning emissions were recognized as the most fundamental sources of $PM_{2.1}$ in Varanasi whereas, both crustal, secondary aerosols including biomass burning emissions were to contribute in coarse particulate. A significant proportion of airborne particulates were also emitted from residential emissions, especially by the use of conventional fuels with energy inefficient cook stoves. Possible transport mechanism of airborne particulates particularly from upper to lower IGP and different local and regional source fields were also identified.

Our analysis was novel by virtue of considering size-segregated aerosols and to recognize its nature and sources over a highly polluted geographical region. Size-segregation in airborne particulate helped us to isolate relative abundance of various chemical species and their associated sources more realistically. Implications of this analysis may be particularly in reducing uncertainty in regional air quality and chemical transport model, providing vital evidence of source specific impacts of particulates to human health and changing climate. However, our analysis also constrains by the unavailability of carbonaceous aerosols (organic and elemental carbon) and particulate-bound carbonate and bicarbonate ions; which could have further strengthen our understanding on abundance and chemistry of airborne particulates.

Author contributions

Nandita Singh: designed the research, experimented, analyzed, reviewed and interpreted the results, drafted the manuscript. **Tirthankar Banerjee:** designed the research, analyzed, reviewed and interpreted the results, drafted the manuscript. **Vishnu Murari:** analyzed. **Karine Deboudt:** analyzed, reviewed and interpreted the results, drafted the manuscript. **Md Firoz Khan:** reviewed and interpreted the results. **RS Singh:** reviewed and interpreted the results. **Mohd Talib Latif:** reviewed and interpreted the results.

Declaration of competing interest

The authors declare that they have no known competing financial interests or personal relationships that could have appeared to influence the work reported in this paper.

Acknowledgements

This research is financially supported by Science and Engineering Research Board, Department of Science and Technology, New Delhi (SR/FTP/ES-52/2014) and ASEAN- India S&T Development Fund, Govt. of India (CRD/2018/000011) under ASEAN- India Collaborative Research and Development Scheme. The research corresponds to a part of doctoral thesis by NS in IESD, BHU. NS

acknowledges Department of Science and Technology Women Scientist scheme for doctoral research (SR/WOS-A/EA-1012/2015), and RSS & TB acknowledge fund from VSSC, Indian Space Research Organization (R&D/SA/ISRO/ChE/19/2006). Authors are thankful to two anonymous reviewers for their constructive suggestions.

Appendix A. Supplementary data

Supplementary data to this article can be found online at https://doi.org/10.1016/j.chemosphere.2020.128030.

References

Banerjee, T., Murari, V., Kumar, M., Raju, M.P., 2015. Source apportionment of airborne particulates through receptor modeling: Indian scenario. Atmos. Res. 164, 167–187.
Begum, B.A., Kim, E., Biswas, S.K., Hopke, P.K., 2004. Investigation of sources of atmospheric aerosol at urban and semi-urban areas in Bangladesh. Atmos. Environ. 38 (19), 3025–3038.
Belis, C.A., Karagulian, F., Larsen, B.R., Hopke, P.K., 2013. Critical review and meta-analysis of ambient particulate matter source apportionment using receptor models in Europe. Atmos. Environ. 69, 94–108.
Bray, C.D., Battye, W., Aneja, V.P., Tong, D.Q., Lee, P., Tang, Y., 2018. Ammonia emissions from biomass burning in the continental United States. Atmos. Environ. 187, 50–61.
Cesari, D., De Benedetto, G.E., Bonasoni, P., Busetto, M., Dinoi, A., Merico, E., Chirizzi, D., Cristofanelli, P., Donateo, A., Grasso, F.M., Marinoni, A., 2018. Seasonal variability of PM2. 5 and PM10 composition and sources in an urban background site in Southern Italy. Sci. Total Environ. 612, 202–213.
Chakraborty, A., Gupta, T., 2010. Chemical characterization and source apportionment of submicron (PM1) aerosol in Kanpur region, India. Aerosol and Air Quality Research 10, 433–445.
Chakraborty, A., Bhattu, D., Gupta, T., Tripathi, S.N., Canagaratna, M.R., 2015. Real-time measurements of ambient aerosols in a polluted Indian city: sources, characteristics, and processing of organic aerosols during foggy and non foggy periods. J. Geophys. Res.: Atmosphere 120 (17), 9006–9019.
Chen, S., Zhao, Y., Zhang, R., 2018. Formation mechanism of atmospheric ammonium bisulfate: hydrogen-bond-promoted nearly barrierless reactions of SO3 with NH3 and H2O. ChemPhysChem 19 (8), 967–972.
Cheng, Y., Engling, G., He, K.B., Duan, F.K., Ma, Y.L., Du, Z.Y., Liu, J.M., Zheng, M., Weber, R.J., 2013. Biomass burning contribution to Beijing aerosol. Atmos. Chem. Phys. 13, 7765–7781.
Chow, J.C., Watson, J.G., Lu, Z., Lowenthal, D.H., Frazier, C.A., Solomon, P.A., Thuillier, R.H., Magliano, K., 1996. Descriptive analysis of PM2. 5 and PM10 at regionally representative locations during SJVAQS/AUSPEX. Atmos. Environ. 30 (12), 2079–2112.
Chowdhury, Z., Zheng, M., Schauer, J.J., Sheesley, R.J., Salmon, L.G., Cass, G.R., Russell, A.G., 2007. Speciation of ambient fine organic carbon particles and source apportionment of PM2. 5 in Indian cities. J. Geophys. Res.: Atmosphere 112 (D15).
Dey, S., Di Girolamo, L., 2011. A decade of change in aerosol properties over the Indian subcontinent. Geophys. Res. Lett. 38 (14).
Dey, S., Tripathi, S.N., Singh, R.P., Holben, B.N., 2004. Influence of dust storms on the aerosol optical properties over the Indo-Gangetic basin. J. Geophys. Res.: Atmosphere 109 (D20).
Didyk, B.M., Simoneit, B.R., Pezoa, L.A., Riveros, M.L., Flores, A.A., 2000. Urban aerosol particles of Santiago, Chile:: organic content and molecular characterization. Atmos. Environ. 34 (8), 1167–1179.
Draxler, R.R., Rolph, G.D., 2003. HYSPLIT (HYbrid Single-Particle Lagrangian Integrated Trajectory) Model Access via NOAA ARL READY Website. NOAA Air Resources Laboratory, Silver Spring http://www. arl. noaa. gov/ready/hysplit4. html.
EPA, US., 1999. National air quality and emissions trends report. Office of Air Quality Planning and Standards.
Fu, P., Kawamura, K., Miura, K., 2011. Molecular characterization of marine organic aerosols collected during a round-the-world cruise. J. Geophys. Res.: Atmosphere 116 (D13).
Fu, P.Q., Kawamura, K., Chen, J., Charriere, B., Sempere, R., 2013. Organic molecular composition of marine aerosols over the Arctic Ocean in summer: contributions of primary emission and secondary aerosol formation. Biogeosciences 10 (2), 653–667.
Fu, P.Q., Kawamura, K., Pavuluri, C.M., Swaminathan, T., Chen, J., 2010. Molecular characterization of urban organic aerosol in tropical India: contributions of primary emissions and secondary photooxidation. Atmos. Chem. Phys. 10 (6), 2663–2689.
Gadi, R., Sharma, S.K., Mandal, T.K., 2019. Source apportionment and health risk assessment of organic constituents in fine ambient aerosols (PM2. 5): a complete year study over National Capital Region of India. Chemosphere 221, 583–596.
Giles, D.M., Holben, B.N., Tripathi, S.N., Eck, T.F., Newcomb, W.W., Slutsker, I., et al., 2011. Aerosol properties over the Indo-Gangetic Plain: a mesoscale perspective from the TIGERZ experiment. J. Geophys. Res.: Atmosphere 116 (D18).
Giri, B., Patel, K.S., Jaiswal, N.K., Sharma, S., Ambade, B., Wang, W., Simonich, S.L.M., Simoneit, B.R., 2013. Composition and sources of organic tracers in aerosol particles of industrial central India. Atmos. Res. 120, 312–324.
Gonzalez, R.O., Strekopytov, S., Amato, F., Querol, X., Reche, C., Weiss, D., 2016. New insights from zinc and copper isotopic compositions into the sources of atmospheric particulate matter from two major European cities. Environ. Sci. Technol. 50 (18), 9816–9824.
Hu, Q.H., Xie, Z.Q., Wang, X.M., Kang, H., Zhang, P., 2013. Levoglucosan indicates high levels of biomass burning aerosols over oceans from the Arctic to Antarctic. Sci. Rep. 3 (1), 1–7.
Jain, S., Sharma, S.K., Vijayan, N., Mandal, T.K., 2020. Seasonal Characteristics of Aerosols (PM2. 5 and PM10) and Their Source Apportionment Using PMF: A Four Year Study over Delhi, India. Environmental Pollution, p. 114337.
Jethva, H., Satheesh, S.K., Srinivasan, J., 2005. Seasonal variability of aerosols over the Indo-Gangetic basin. J. Geophys. Res.: Atmosphere 110 (D21).
Jimenez, J.L., Canagaratna, M.R., Donahue, N.M., Prevot, A.S.H., Zhang, Q., Kroll, J.H., DeCarlo, P.F., Allan, J.D., Coe, H., Ng, N.L., Aiken, A.C., 2009. Evolution of organic aerosols in the atmosphere. Science 326 (5959), 1525–1529.
Kang, M., Fu, P., Aggarwal, S.G., Kumar, S., Zhao, Y., Sun, Y., Wang, Z., 2016. Size distributions of n-alkanes, fatty acids and fatty alcohols in springtime aerosols from New Delhi, India. Environ. Pollut. 219, 957–966.
Kaskaoutis, D.G., Kumar, S., Sharma, D., Singh, R.P., Kharol, S.K., Sharma, M., Singh, A.K., Singh, S., Singh, A., Singh, D., 2014. Effects of crop residue burning on aerosol properties, plume characteristics, and long-range transport over northern India. J. Geophys. Res.: Atmosphere 119 (9), 5424–5444.
Kawamura, K., Gagosian, R.B., 1987. Implications of ω-oxocarboxylic acids in the remote marine atmosphere for photo-oxidation of unsaturated fatty acids. Nature 325 (6102), 330–332.
Kawamura, K., Yasui, O., 2005. Diurnal changes in the distribution of dicarboxylic acids, ketocarboxylic acids and dicarbonyls in the urban Tokyo atmosphere. Atmos. Environ. 39 (10), 1945–1960.
Khan, M.F., Latif, M.T., Saw, W.H., Amil, N., Nadzir, M.S.M., Sahani, M., Tahir, N.M., Chung, J.X., 2016. Fine particulate matter in the tropical environment: monsoonal effects, source apportionment, and health risk assessment. Atmos. Chem. Phys. 16 (2), 597–617.
Kirillova, E.N., Sheesley, R.J., Andersson, A., Gustafsson, O., 2010. Natural abundance 13C and 14C analysis of water-soluble organic carbon in atmospheric aerosols. Anal. Chem. 82 (19), 7973–7978.
Kukutschová, J., Moravec, P., Tomášek, V., Matějka, V., Smolík, J., Schwarz, J., Seidlerová, J., Šafářová, K., Filip, P., 2011. On airborne nano/micro-sized wear particles released from low-metallic automotive brakes. Environ. Pollut. 159 (4), 998–1006.
Kulshrestha, A., Satsangi, P.G., Masih, J., Taneja, A., 2009. Metal concentration of PM2. 5 and PM10 particles and seasonal variations in urban and rural environment of Agra, India. Sci. Total Environ. 407 (24), 6196–6204.
Kumar, M., Parmar, K.S., Kumar, D.B., Mhawish, A., Broday, D.M., Mall, R.K., Banerjee, T., 2018. Long-term aerosol climatology over Indo-Gangetic Plain: trend, prediction and potential source fields. Atmos. Environ. 180, 37–50.
Kumar, M., Raju, M.P., Singh, R.K., Singh, A.K., Singh, R.S., Banerjee, T., 2017. Wintertime characteristics of aerosols over middle Indo-Gangetic Plain: vertical profile, transport and radiative forcing. Atmos. Res. 183, 268–282.
Kumar, M., Tiwari, S., Murari, V., Singh, A.K., Banerjee, T., 2015. Wintertime characteristics of aerosols at middle Indo-Gangetic Plain: impacts of regional meteorology and long range transport. Atmos. Environ. 104, 162–175.
Lelieveld, J., Evans, J.S., Fnais, M., Giannadaki, D., Pozzer, A., 2015. The contribution of outdoor air pollution sources to premature mortality on a global scale. Nature 525 (7569), 367–371.
Li, J., Wang, G., Aggarwal, S.G., Huang, Y., Ren, Y., Zhou, B., Singh, K., Gupta, P.K., Cao, J., Zhang, R., 2014. Comparison of abundances, compositions and sources of elements, inorganic ions and organic compounds in atmospheric aerosols from Xi'an and New Delhi, two megacities in China and India. Sci. Total Environ. 476, 485–495.
Martin, R.V., Brauer, M., van Donkelaar, A., Shaddick, G., Narain, U., Dey, S., 2019. No one knows which city has the highest concentration of fine particulate matter. Atmos. Environ. X (3), 100040.
Mhawish, A., Banerjee, T., Broday, D.M., Misra, A., Tripathi, S.N., 2017. Evaluation of MODIS Collection 6 aerosol retrieval algorithms over Indo-Gangetic Plain: implications of aerosols types and mass loading. Remote Sens. Environ. 201, 297–313.
Miyazaki, Y., Aggarwal, S.G., Singh, K., Gupta, P.K., Kawamura, K., 2009. Dicarboxylic acids and water-soluble organic carbon in aerosols in New Delhi, India, in winter: characteristics and formation processes. J. Geophys. Res.: Atmosphere 114 (D19).
Mhawish, A., Banerjee, T., Sorek-Hamer, M., Bilal, M., Lyapustin, A., Chatfield, R.B., Broday, D., 2020. Estimation of high-resolution PM2. 5 over Indo-Gangetic Plain by fusion of satellite data, meteorology, and land use variables. Environ. Sci. Technol. 54 (13), 7891–7900.
Murari, V., Kumar, M., Barman, S.C., Banerjee, T., 2015. Temporal variability of MODIS aerosol optical depth and chemical characterization of airborne particulates in Varanasi, India. Environ. Sci. Pollut. Control Ser. 22 (2), 1329–1343.
Murari, V., Kumar, M., Mhawish, A., Barman, S.C., Banerjee, T., 2017. Airborne particulate in Varanasi over middle Indo-Gangetic Plain: variation in particulate types and meteorological influences. Environ. Monit. Assess. 189 (4), 157.
Murari, V., Singh, N., Ranjan, R., Singh, R.S., Banerjee, T., 2020. Source

apportionment and health risk assessment of airborne particulates over central Indo-Gangetic Plain. Chemosphere 257, 127145.
Paatero, P., Tapper, U., 1994. Positive matrix factorization: a non-negative factor model with optimal utilization of error estimates of data values. Environmetrics 5 (2), 111–126.
Pant, P., Harrison, R.M., 2012. Critical review of receptor modelling for particulate matter: a case study of India. Atmos. Environ. 49, 1–12.
Pavuluri, C.M., Kawamura, K., Swaminathan, T., 2010. Water-soluble organic carbon, dicarboxylic acids, ketoacids, and α-dicarbonyls in the tropical Indian aerosols. J. Geophys. Res.: Atmosphere 115 (D11).
Querol, X., Alastuey, A., Rodriguez, S., Plana, F., Ruiz, C.R., Cots, N., Massagué, G., Puig, O., 2001. PM10 and PM2. 5 source apportionment in the Barcelona Metropolitan area, Catalonia, Spain. Atmos. Environ. 35 (36), 6407–6419.
Ramanathan, V.C.P.J., Crutzen, P.J., Kiehl, J.T., Rosenfeld, D., 2001. Aerosols, climate, and the hydrological cycle. Science 294 (5549), 2119–2124.
Rasheed, A., Aneja, V.P., Aiyyer, A., Rafique, U., 2015. Measurement and analysis of fine particulate matter (PM2. 5) in urban areas of Pakistan. Aerosol and Air Quality Research 15 (2), 426–439.
Ren, L., Fu, P., He, Y., Hou, J., Chen, J., Pavuluri, C.M., Sun, Y., Wang, Z., 2016. Molecular distributions and compound-specific stable carbon isotopic compositions of lipids in wintertime aerosols from Beijing. Sci. Rep. 6, 27481.
Rogge, W.F., Medeiros, P.M., Simoneit, B.R., 2006. Organic marker compounds for surface soil and fugitive dust from open lot dairies and cattle feedlots. Atmos. Environ. 40 (1), 27–49.
Seinfeld, J.H., Bretherton, C., Carslaw, K.S., Coe, H., DeMott, P.J., Dunlea, E.J., Feingold, G., Ghan, S., Guenther, A.B., Kahn, R., Kraucunas, I., 2016. Improving our fundamental understanding of the role of aerosol– cloud interactions in the climate system. Proc. Natl. Acad. Sci. Unit. States Am. 113 (21), 5781–5790.
Seinfeld, J.H., Pandis, S.N., 2016. Atmospheric Chemistry and Physics: From Air Pollution to Climate Change. John Wiley & Sons.
Sen, A., Abdelmaksoud, A.S., Ahammed, Y.N., Banerjee, T., Bhat, M.A., Chatterjee, A., et al., 2017. Variations in particulate matter over Indo-Gangetic Plains and Indo-Himalayan Range during four field campaigns in winter monsoon and summer monsoon: role of pollution pathways. Atmos. Environ. 154, 200–224.
Sen, A., Ahammed, Y.N., Arya, B.C., Banerjee, T., Begam, G.R., Baruah, B.P., Chatterjee, A., Choudhuri, A.K., Dhir, A., Das, T., Dhyani, P.P., 2014. Atmospheric fine and coarse mode aerosols at different environments of India and the Bay of Bengal during winter-2014: implications of a coordinated campaign. Mapan 29 (4), 273–284.
Sharma, S.K., Mandal, T.K., Saxena, M., Sharma, A., Gautam, R., 2014. Source apportionment of PM10 by using positive matrix factorization at an urban site of Delhi, India. Urban climate 10, 656–670.
Sharma, S.K., Mandal, T.K., Srivastava, M.K., Chatterjee, A., Jain, S., Saxena, M., Singh, B.P., Sharma, A., Adak, A., Ghosh, S.K., 2016. Spatio-temporal variation in chemical characteristics of PM 10 over Indo Gangetic plain of India. Environ. Sci. Pollut. Control Ser. 23 (18), 18809–18822.
Shukla, S.P., Sharma, M., 2008. Source apportionment of atmospheric PM10 in Kanpur, India. Environ. Eng. Sci. 25 (6), 849–862.
Singh, D.K., Gupta, T., 2016. Role of transition metals with water soluble organic carbon in the formation of secondary organic aerosol and metallo-organics in PM1 sampled during post monsoon and pre-winter time. J. Aerosol Sci. 94, 56–69.
Singh, N., Banerjee, T., Raju, M.P., Deboudt, K., Sorek-Hamer, M., Singh, R.S., Mall, R.K., 2018. Aerosol chemistry, transport, and climatic implications during extreme biomass burning emissions over the Indo-Gangetic Plain. Atmos. Chem. Phys. 18 (19), 14197–14215.
Singh, N., Mhawish, A., Deboudt, K., Singh, R.S., Banerjee, T., 2017a. Organic aerosols over Indo-Gangetic Plain: sources, distributions and climatic implications. Atmos. Environ. 157, 59–74.
Singh, N., Murari, V., Kumar, M., Barman, S.C., Banerjee, T., 2017b. Fine particulates over South Asia: review and meta-analysis of PM2. 5 source apportionment through receptor model. Environ. Pollut. 223, 121–136.
Sorathia, F., Rajput, P., Gupta, T., 2018. Dicarboxylic acids and levoglucosan in aerosols from Indo-Gangetic Plain: inferences from day night variability during wintertime. Sci. Total Environ. 624, 451–460.
Tan, J.H., Duan, J.C., Chen, D.H., Wang, X.H., Guo, S.J., Bi, X.H., Sheng, G.Y., He, K.B., Fu, J.M., 2009. Chemical characteristics of haze during summer and winter in Guangzhou. Atmos. Res. 94 (2), 238–245.
Theodosi, C., Grivas, G., Zarmpas, P., Chaloulakou, A., Mihalopoulos, N., 2011. Mass and chemical composition of size-segregated aerosols (PM 1, PM 2.5, PM 10) over Athens, Greece: local versus regional sources. Atmos. Chem. Phys. 11 (22), 11895–11911.
Tian, M., Wang, H., Chen, Y., Yang, F., Zhang, X., Zou, Q., Zhang, R., Ma, Y., He, K., 2016. Characteristics of aerosol pollution during heavy haze events in Suzhou, China. Atmos. Chem. Phys. 16 (11), 7357-7357.
Viana, M., Kuhlbusch, T.A.J., Querol, X., Alastuey, A., Harrison, R.M., Hopke, P.K., Hitzenberger, R., 2008. Source apportionment of particulate matter in Europe: a review of methods and results. J. Aerosol Sci. 39, 827–849.
Villalobos, A.M., Amonov, M.O., Shafer, M.M., Devi, J.J., Gupta, T., Tripathi, S.N., Rana, K.S., Mckenzie, M., Bergin, M.H., Schauer, J.J., 2015. Source apportionment of carbonaceous fine particulate matter (PM2. 5) in two contrasting cities across the Indo–Gangetic Plain. Atmospheric Pollution Research 6 (3), 398–405.
Vinjamuri, K.S., Mhawish, A., Banerjee, T., Sorek-Hamer, M., Broday, D.M., Mall, R.K., Latif, M.T., 2020. Vertical distribution of smoke aerosols over upper Indo-Gangetic Plain. Environ. Pollut. 257, 113377.
Wan, X., Kang, S., Li, Q., Rupakheti, D., Zhang, Q., Guo, J., Chen, P., Tripathee, L., Rupakheti, M., Panday, A.K., Wang, W., 2017. Organic molecular tracers in the atmospheric aerosols from Lumbini, Nepal, in the northern Indo-Gangetic Plain: influence of biomass burning. Atmos. Chem. Phys. 17 (14), 8867–8885.
Wang, Y.Q., Zhang, X.Y., Draxler, R.R., 2009. TrajStat: GIS-based software that uses various trajectory statistical analysis methods to identify potential sources from long-term air pollution measurement data. Environ. Model. Software 24 (8), 938–939.
Weagle, C.L., Snider, G., Li, C., van Donkelaar, A., Philip, S., Bissonnette, P., Burke, J., Jackson, J., Latimer, R., Stone, E., Abboud, I., 2018. Global sources of fine particulate matter: interpretation of PM2. 5 chemical composition observed by SPARTAN using a global chemical transport model. Environ. Sci. Technol. 52 (20), 11670–11681.